

# Quantum-thermodynamic enhancements in continuous thermal machines require energetic coherence

José A. Almanza-Marrero<sup>1</sup> and Gonzalo Manzano<sup>1</sup>

<sup>1</sup>*Institute for Cross-Disciplinary Physics and Complex Systems IFISC (UIB-CSIC),  
Campus Universitat Illes Balears, E-07122 Palma de Mallorca, Spain*

(Dated: March 29, 2024)

Quantum coherence has been shown to impact the operational capabilities of quantum systems performing thermodynamic tasks in a significant way, and yet the possibility of genuine coherence-enhanced thermodynamic operation remains unclear. Here we show that only the presence of energetic coherence—coherence between levels with different energies—in steady-state quantum thermal machines can lead to genuine thermodynamic advantage. On the other hand, engines showing coherence between degenerate levels, or subjected to noise-induced coherence, are shown to be systematically outperformed by classical stochastic engines using exactly the same set of (incoherent) resources. We illustrate our results with three prototypical models of heat engines and refrigerators and employ multi-objective optimization techniques to characterize quantum-enhanced regimes in connection with the thermodynamic uncertainty relation.

## I. INTRODUCTION

The determination of the interplay between quantum coherence—i.e. the ability of quantum systems to exist in superpositions of multiple states—and thermodynamic operation, constitutes one of the main challenges in quantum thermodynamics, attracting increasing attention during the last decade [1, 2]. One of the main approaches to explore this link, in line with the original spirit of thermodynamics, has consisted in the construction and analysis of minimal models of quantum thermal machines showing different types of coherent evolution [3–9]. These machines consist of a quantum system—the working medium—composed by few energy levels or qubits which, by coupling to thermal baths at different temperatures and external work sources, are able to perform useful thermodynamic tasks, such as work extraction, heat pumping, or refrigeration. Recent advances in the manipulation and control of quantum systems in the laboratory allowed the implementation of first prototypes, where the basic principles of these models can be mapped to realistic devices in platforms ranging from ion-traps [10, 11] to NV centers in diamond [12], just to mention a few of them [1, 13].

Since the pioneering works of Scully *et al.* introducing a photo-Carnot engine [14], quantum coherence has been claimed to increase the power output or efficiency of many different types of quantum heat engines and refrigerators. Such improvements are particularly relevant in the case of continuous machines working in steady-state conditions [15], which in principle require less control of the dynamics and couplings with reservoirs. Particularly relevant examples include power-enhancements by noise-induced coherence in lasers, photocell engines, or quantum dots engines [16–18] (with applications in photosynthetic light harvesting [19]), or by input external coherent fields [9, 12], as well as cooling boosts by degenerate coherence in local models of quantum absorption refrigerators [20–22]. In all such cases, coherence has been found

to play a positive role in the output mechanism, eventually leading to an increased ability of the machine for work extraction or refrigeration. However, since all such output mechanisms are model-dependent, it remains unclear whether the performance shown by these machines cannot be achieved by other equivalent classical models [9, 22, 23], so that a truly quantum thermodynamic advantage can be identified. Given the possibility of implementation of these models in the laboratory and their potential applications, clarifying this point becomes an urgent and crucial point to the field.

In this paper we show how to identify genuine coherence-induced quantum thermodynamic advantage and how to quantitatively characterize it in steady-state quantum thermal machines by combining three main ingredients. The first one is the systematic construction of thermodynamically-equivalent classical thermal machines that are able to produce the same average currents than their quantum-coherent counterparts, while using exactly the same amount of incoherent resources (essentially bath temperatures and energy structure). However, even if same average currents can be reproduced by classical models, fluctuations as captured by the variance of the currents might present significant differences. The comparison of fluctuations in the output currents (reliability of the machine) with respect to the classical counterpart is henceforth the second necessary ingredient in our analysis. This is connected with violations in the so-called thermodynamic uncertainty relation (TUR) [24–26], which provides a universal trade-off relation between power, efficiency, and output reliability for any classical Markovian thermal machine operating at steady-state conditions [27]. The TUR sets up a model-independent limit in the maximum reliability achievable by any classical machine at a given power output and efficiency. Hence the observation of TUR violations in quantum Markovian machines working in steady-state conditions [28–33] may be considered as an unambiguous witness of a quantum thermodynamic signature. Nev-

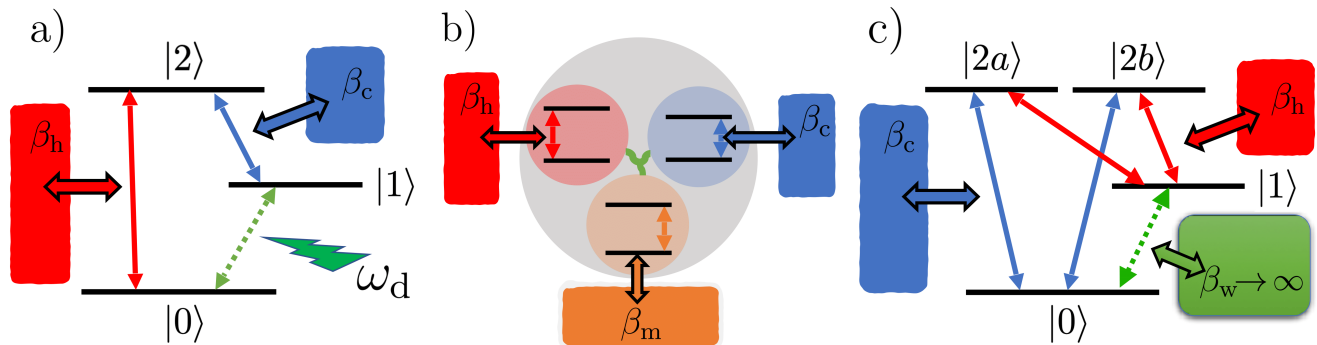


FIG. 1. Schematic representation of (a) the coherent three-level amplifier coupled to baths at hot  $\beta_h$  and cold  $\beta_c$  temperatures and coherent external driving, (b) the three-qubit autonomous (absorption) refrigerator where each qubit is locally coupled to baths at hot, cold, and intermediate temperatures  $\beta_m$ , and (c) the noise-induced-coherence machine showing collective jumps induced by the baths at hot and cold temperatures, together with a classical work source given by an infinite-temperature bath.

ertheless, the violation of the TUR in specific parameter regimes is not yet a sufficient (nor necessary) condition for ensuring a practical quantum-thermodynamic advantage in thermal machines, since these parameter regimes may be far from optimal performance. The third ingredient that we employ here is the use of multi-objective optimization techniques (Pareto optimization) [34–39] to actually confirm enhanced stability (precision), power output or efficiency, with respect to classical thermodynamically-equivalent machines, in relevant (optimal) regimes of operation of the machine, such as maximum power conditions.

Although our analysis is applicable to a broad class of steady-state quantum thermal machines, we employ three well-known (prototypical) models showing coherent-induced evolution (see Fig. 1), each corresponding to one of the three possible types of coherence that can arise in the working medium when approaching the steady state: (a) coherence between different energy levels (energetic coherence) induced by external driving, (b) coherence between levels with degenerate energies induced by internal Hamiltonian couplings, and (c) noise-induced coherence on degenerate levels induced by the reservoir. Our results show that only in the case of energetic coherence (case a) a practical quantum-thermodynamic advantage can be unambiguously identified, leading to enhanced optimal regimes not allowed by any equivalent classical engine using the same amount of thermodynamic resources. On the contrary, coherence in degenerate energy levels (cases b and c) can only lead to disadvantages in the performance, even in cases where the quantum machine dynamics contains intrinsic quantum features.

This paper is organized as follows: Sec. II introduces the different thermal machine models in detail. Sec. III discusses how to characterize the thermodynamic performance in such systems. In Sec. IV, we describe the concept of classical equivalent machines and provide a general recipe for constructing them in the presence of

different types of coherence. Sec. V A demonstrates that, in the presence of energetic coherence, quantum enhancements can be achieved with respect to classical equivalent machines. Sec. V B demonstrate instead the disadvantages of quantum machines with non-energetic (i.e. degenerate) coherence compared to their classical counterparts. In Sec. VI, we optimize both quantum and classical thermal machines and compare their optimal solutions. Finally, Sec. VII provides a summary and conclusions of our main results.

## II. QUANTUM THERMAL MACHINES MODELS

We consider thermal machines running continuously in a steady-state regime described as open quantum systems interacting with two or more thermal baths at different temperatures. The machine system has  $N$  energy levels, some of which may be degenerate or not, and interconnected through incoherent transitions mediated by the baths. Moreover, we consider the possibility of one or more coherent interactions arising as a consequence of one of the three following sources (see Fig. 1): (a) external driving by a classical field (such as in quantum heat engine models of masers and lasers [3–5]); (b) internal Hamiltonian interactions between subsystems in few-body machines (e.g. machines composed by several interacting qubits [6] or harmonic oscillators [7]), and (c) noise-induced coherence caused from collective dissipation acting on two or more resonant transitions (as in some light-harvesting complexes [19] and synthetic heat engine models [17]).

The general Hamiltonian of the machine can be generically written as the sum of two terms:

$$H = H_0 + V(t), \quad (1)$$

where  $H_0 = \sum_{i=0}^{N-1} \epsilon_i |i\rangle \langle i|$  is a local Hamiltonian describing  $N$  energy levels with  $\epsilon_0 \leq \epsilon_1 \leq \dots \leq \epsilon_{N-1}$ , and

$V(t)$  is a (eventually time-dependent) term capturing coherent transitions between them. It can either represent an external field periodically driving a transition in  $H_0$ , or, in the case of multipartite systems, the internal interaction among machine constituents. An important feature of this interaction Hamiltonian is that it does not severely modify the energy level structure of the system, so that it can be treated as a perturbation to the local Hamiltonian  $H_0$  (i.e.  $|V| \ll |H_0|$ ). On the other hand, for thermal machines using only noise-induced coherence we will typically have  $V(t) = 0$  and then  $H = H_0$ , since that type of coherence appears solely from the effect of the baths. Without loss of generality, we set to zero the ground-state energy of the machine,  $\epsilon_0 \equiv 0$ .

We are interested in the quantum Markovian dynamics of the machine in the weak coupling regime. Under Born-Markov and secular approximations, it is possible to describe the evolution of the machine state  $\rho(t)$  in terms of a quantum master equation in Lindblad form [40–44]:

$$\frac{d\rho(t)}{dt} = \mathcal{L}(\rho) = -i[H(t), \rho(t)] + \sum_{r=1}^R \sum_{k=\uparrow\downarrow} \mathcal{D}_k^{(r)}[\rho(t)], \quad (2)$$

where  $H(t)$  is given in Eq. (1) and  $\mathcal{D}_k^{(r)}(\rho)$  denote the so-called dissipators, taking into account the effects of dissipative process  $k$  from thermal reservoir  $r$  on the system. These dissipators are given in terms of Lindblad operators  $L_k^{(r)}$  associated to each reservoir:

$$\mathcal{D}_k^{(r)}[\rho(t)] := \left( L_k^{(r)} \rho L_k^{(r)\dagger} - \frac{1}{2} \left\{ L_k^{(r)\dagger} L_k^{(r)}, \rho \right\} \right). \quad (3)$$

The Lindblad operators  $L_k^{(r)}$  here induce jumps between the  $H_0$  levels with fixed energy gap  $\Delta\epsilon_k = \pm\Delta\epsilon_r$  determined by bath  $r$ , and verify  $[H_0, L_k^{(r)}] = -\Delta\epsilon_k L_k^{(r)}$ . They can be written in general as:

$$L_k^{(r)} = \sum_{i,j} \alpha_{ij}^k \sqrt{\gamma_{ij}} |j\rangle \langle i|, \quad (4)$$

with  $\alpha_{ij}^k = 1$  if  $\epsilon_j - \epsilon_i = \Delta\epsilon_k$  and 0 otherwise. In the case of non-degenerate transitions, the above operators reduce to simple jumps  $L_k^{(r)} = \sqrt{\gamma_{ij}} |j\rangle \langle i|$  between energy levels  $i \rightarrow j$ . However, the operators in Eq. (4) can also describe collective jumps where two or more transitions with same (degenerate) gap  $\Delta\epsilon_k$  in  $H_0$  may occur simultaneously, e.g.  $i \rightarrow j$  and  $i \rightarrow j'$  if  $\epsilon_j = \epsilon_{j'}$ . In any case, every transition is connected to a single thermal bath, the rates  $\gamma_{ij} \geq 0$  being time-independent and verifying the local detailed balance relation  $\gamma_{ij} = \gamma_{ji} e^{-\beta_r(\epsilon_j - \epsilon_i)}$ , with  $\beta_r = 1/k_B T_r$  the inverse temperature of the bath  $r$  and  $k_B$  Boltzmann's constant. In the long-time limit, the evolution dictated by Eq. (3) converges to a steady-state, verifying  $\mathcal{L}(\pi) = 0$ , where we denote  $\pi(t)$  the steady state density operator. We notice that, due to the presence of the time-dependent Hamiltonian  $V(t)$ , the steady state can show a (residual) periodic time-dependence in the

phase in the Schrödinger picture, which disappears when moving to a rotating frame.

Although the results we present here can be applied to any model of quantum thermal machine whose evolution can be described within the general framework introduced above, in this paper we will mainly focus on three representative and well-known models of quantum thermal machines, as illustrated in Fig. 1. They lead to three different types of coherent evolution respectively: the coherent three-level maser (Fig. 1a) which induces energetic coherence in the  $H_0$  basis; the three-qubit autonomous quantum refrigerator (Fig. 1b), leading to Hamiltonian-induced coherence in a degenerate subspace of  $H_0$ , and the noise-induced-coherence engine (Fig. 1c), showing coherence between degenerate levels induced by collective bath transitions.

### A. Coherent three-level amplifier

The three-level maser or amplifier, as initially introduced by Scovil and Schulz-DuBois in Ref. [3], is one of the simplest models of a thermal machine, capable of serving either as a heat engine or a refrigerator depending on the configuration of system parameters [45, 46]. The characteristics and performance of this model has been largely studied [1, 4, 5, 15, 30, 46–49] owing to its simplicity and versatile functionality, and a first experimental implementation has been reported in Ref. [12]. It stands as a main example of a thermal machine where coherence among non-degenerate energy levels is supported in the steady state, suggesting the appearance of regimes where quantum-enhanced thermodynamic operation can be achieved [9] (for a critical view of such quantum-enhanced performance see e.g. Ref. [23]).

The machine system contains three discrete energy levels and an external driving field acting on its lower transition, as depicted in Fig. 1a. The Hamiltonian of the system can be written in this case as:

$$H = \epsilon_1 |1\rangle \langle 1| + \epsilon_2 |2\rangle \langle 2| + V(t), \quad (5)$$

with bare Hamiltonian  $H_0 := \epsilon_1 |1\rangle \langle 1| + \epsilon_2 |2\rangle \langle 2|$  time dependent driving Hamiltonian  $V(t) = g(e^{-i\omega_d t} |0\rangle \langle 1| + \text{h.c.})$  resonant with the first energy gap, i.e.  $\omega_d \equiv \epsilon_1$ , and where  $g$  is the external driving field strength. In the absence thermal baths, this driving field generates Rabi-like oscillations within the first two levels of the machine,  $|0\rangle$  and  $|1\rangle$ , at frequency  $g$ .

The two remaining transitions of the three-level system are further weakly coupled to two thermal baths at different inverse temperatures, denoted as cold and hot ( $\beta_c \geq \beta_h$ ), typically modeled as bosonic reservoirs. They lead to four incoherent jumps described by Lindblad operators:

$$\begin{aligned} L_{\downarrow}^{(c)} &= \sqrt{\gamma_{21}} |1\rangle \langle 2|; & L_{\uparrow}^{(c)} &= \sqrt{\gamma_{12}} |2\rangle \langle 1|, \\ L_{\downarrow}^{(h)} &= \sqrt{\gamma_{20}} |0\rangle \langle 2|; & L_{\uparrow}^{(h)} &= \sqrt{\gamma_{02}} |2\rangle \langle 0|, \end{aligned} \quad (6)$$

with rates  $\gamma_{21} = \gamma_c(\bar{n}_c + 1)$  and  $\gamma_{12} = \gamma_c\bar{n}_c$  associated respectively to the emission and absorption of energy quanta  $\Delta\epsilon_c = \epsilon_2 - \epsilon_1$  into the cold reservoir at  $\beta_c$ . Similarly  $\gamma_{20} = \gamma_h(\bar{n}_h + 1)$  and  $\gamma_{02} = \gamma_h\bar{n}_h$  stand for emission and absorption of energy quanta  $\Delta\epsilon_h = \epsilon_2$  into the hot reservoir at temperature  $\beta_h$ . Here  $\gamma_r$  denotes the spontaneous emission rate for bath  $r = c, h$  and  $\bar{n}_r = (e^{\beta_r\Delta\epsilon_r} - 1)^{-1}$  is the average number of thermal photons with frequency  $\Delta\epsilon_r$  in the baths.

As commented before, since we are treating the interaction Hamiltonian as a perturbation, our analysis will be limited to the weak driving regime. In this regime, it is possible to extract the time dependence of the system's Hamiltonian by moving to a rotating frame (interaction picture with respect to  $H_0$ ). This transformation leads to the following form of the master equation (2):

$$\frac{d\rho'}{dt} = -i[V_I, \rho'] + \sum_{r=c,h} \sum_{k=\downarrow,\uparrow} \mathcal{D}_k^{(r)}[\rho'], \quad (7)$$

where  $\rho' = e^{iH_0t}\rho e^{-iH_0t}$  and the driving Hamiltonian in the interaction picture appearing in the Lindblad equation has the simpler form  $V_I = g(|0\rangle\langle 1| + |1\rangle\langle 0|)$ .

### B. Three-qubit autonomous refrigerator

This fridge model was first presented in Ref. [6] and consist of one of the smallest thermal machines models using a multipartite system (see Fig. 1b). It pertains to the class of autonomous quantum refrigerators [8, 50, 51], also called quantum absorption refrigerators [7, 21, 52–55]. It consists of three qubits with different energy gaps, each of them locally coupled to a corresponding thermal baths at a different temperature. A weak three-body energy-preserving Hamiltonian interaction among the qubits allows the generation of heat currents between the three reservoirs that ultimately power thermodynamic tasks such as heat pumping or refrigeration [8]. Different platforms for the actual implementation of this or closely related models in the lab has been proposed using quantum dots [56], optical systems [57], QED architectures [58] and trapped ions [11]. In this multipartite setup, genuine quantum features such as quantum entanglement [20] and discord [52] have been analyzed, suggesting the possibility of boosting the fridge performance by quantum correlations in some operational regimes [20].

The Hamiltonian of the three-qubit working substance here reads:

$$H = H_1 + H_2 + H_3 + V, \quad (8)$$

where we identify  $H_0 = \sum_i H_i$  with  $H_i = \epsilon_i |1\rangle\langle 1|_i$  the (bare) Hamiltonians of each individual qubit and  $V = g(|101\rangle\langle 010| + |010\rangle\langle 101|)$  is a three-body interaction Hamiltonian allowing the qubits to exchange energy (notice the use of the simplified notation  $|101\rangle \equiv$

$|1\rangle_1|0\rangle_2|1\rangle_3$ , etc.). Here above  $g \ll \epsilon_i$ , ensures that the interaction can be treated as a perturbation to the bare three-qubit Hamiltonian  $H_0$ .

Importantly, by assuming the resonance condition  $\epsilon_3 = \epsilon_2 - \epsilon_1$ , the three qubit interaction verifies strict energy preservation between the qubits, that is  $[V, H_1 + H_2 + H_3] = 0$ , ensuring that the energy exchanges among the fridge qubits occur without the need of any extra source of energy or control, i.e. preserving the autonomy of the model. At difference from other autonomous fridges, such as single-qutrit fridges [46], this model exhibits steady-state coherence between degenerate energy levels  $|101\rangle$  and  $|010\rangle$  due to the presence of the interaction  $V$  [6], which ultimately leads to entanglement among different partitions involving the qubits [20].

In this case all the transitions are mediated by the reservoirs, with either cold, medium or hot temperatures ( $\beta_c \geq \beta_m \geq \beta_h$ ). Since each qubit  $i$  is locally coupled only to a single bath at inverse temperature  $\beta_i$ , and the interaction  $V$  is weak, the master equation (2) adopts a local form [42–44], with six incoherent jumps described by Lindblad operators promoting local jumps in each qubit:

$$\begin{aligned} L_{\downarrow}^{(c)} &= \sqrt{\gamma_{10}^c} |0\rangle\langle 1|_1 \otimes \mathbb{1}_2 \otimes \mathbb{1}_3, \\ L_{\downarrow}^{(m)} &= \sqrt{\gamma_{10}^m} \mathbb{1}_1 \otimes |0\rangle\langle 1|_2 \otimes \mathbb{1}_3, \\ L_{\downarrow}^{(h)} &= \sqrt{\gamma_{10}^h} \mathbb{1}_1 \otimes \mathbb{1}_2 \otimes |0\rangle\langle 1|_3, \end{aligned} \quad (9)$$

together with the opposite jumps,  $L_{\uparrow}^{(r)} = e^{-\beta_r\Delta\epsilon_r/2} L_{\downarrow}^{(r)\dagger}$ , for  $r = c, m, h$ . The rates  $\gamma_{10}^c = \gamma_c(\bar{n}_c + 1)$  and  $\gamma_{01}^c = \gamma_c\bar{n}_c$  are associated respectively to the emission and absorption of energy quanta  $\Delta\epsilon_c = \epsilon_1$  into the cold reservoir at  $\beta_c$ . Similarly we have  $\gamma_{10}^m = \gamma_m(\bar{n}_m + 1)$  and  $\gamma_{01}^m = \gamma_m\bar{n}_m$  for the emission and absorption of energy quanta  $\Delta\epsilon_m = \epsilon_2$  into the medium reservoir at temperature  $\beta_m$ , as well as  $\gamma_{10}^h = \gamma_h(\bar{n}_h + 1)$  and  $\gamma_{01}^h = \gamma_h\bar{n}_h$  for the emission and absorption of energy quanta  $\Delta\epsilon_h = \epsilon_3$  into the hot reservoir at temperature  $\beta_h$ .

### C. Noise-induced-coherence machine

A final set of continuous thermal machines models showing quantum effects, which we collectively dub noise-induced-coherence (NIC) machines, were first presented in a series of papers by Scully *et al.* [16, 19, 59]. In these machines, degenerate levels in the energy spectrum are combined with a collective action of the baths on the system transitions to generate coherence in the steady state [60, 61]. The operation and performance of these kind of machines has been extensively investigated within the context of quantum thermal machines [17, 18, 22, 48, 62–68], pointing to enhancements in the power output for adequate operational regimes.

A notable example of this coherence is found in a 4-level absorption refrigerator, whose thermodynamics have been examined in previous studies [66, 68, 69]. In

this system, two of the levels possess the same energy, as depicted in Fig. 1c. These levels are subjected to the influence of two distinct thermal baths, the action of both of which results in the emergence of horizontal coherences that persist in the system's steady state. The system's Hamiltonian in this case is as follows

$$H = \epsilon_1 |1\rangle \langle 1| + \epsilon_2 (|2a\rangle \langle 2a| + |2b\rangle \langle 2b|) = H_0. \quad (10)$$

In this case all the transitions are mediated by the reservoirs at cold, hot and “work” temperatures ( $\beta_c \geq \beta_h > \beta_w \rightarrow 0$ ). To represent these transitions we will have six different incoherent jumps, two of them consisting of individual jumps  $L_{\downarrow}^{(w)} = \sqrt{\gamma_{10}} |0\rangle \langle 1|$  and  $L_{\uparrow}^{(w)} = \sqrt{\gamma_{01}} |1\rangle \langle 0|$ , and the other four refer to collective transitions:

$$\begin{aligned} L_{\downarrow}^{(c)} &= \sqrt{\gamma_{a1}} |1\rangle \langle 2a| + \sqrt{\gamma_{b1}} |1\rangle \langle 2b|, \\ L_{\uparrow}^{(c)} &= \sqrt{\gamma_{1a}} |2a\rangle \langle 1| + \sqrt{\gamma_{1b}} |2b\rangle \langle 1|, \\ L_{\downarrow}^{(h)} &= \sqrt{\gamma_{a0}} |0\rangle \langle 2a| + \sqrt{\gamma_{b0}} |0\rangle \langle 2b|, \\ L_{\uparrow}^{(h)} &= \sqrt{\gamma_{0a}} |2a\rangle \langle 0| + \sqrt{\gamma_{0b}} |2b\rangle \langle 0|, \end{aligned} \quad (11)$$

with rates  $\gamma_{i1} = \gamma_c^i (\bar{n}_c + 1)$  and  $\gamma_{1i} = \gamma_c^i \bar{n}_c$  for  $i = a, b$ , associated respectively to the emission and absorption of energy quanta  $\Delta\epsilon_c = \epsilon_2 - \epsilon_1$  into the cold reservoir at  $\beta_c$ , and similarly  $\gamma_{i0} = \gamma_h^i (\bar{n}_h + 1)$  and  $\gamma_{0i} = \gamma_h^i \bar{n}_h$  for  $i = a, b$ , is associated with emission and absorption of energy quanta  $\Delta\epsilon_h = \epsilon_2$  into the hot reservoir at temperature  $\beta_h$ . Finally, since the “work” bath is at an infinite temperature i.e.  $\beta_w \rightarrow 0$  the rates associated to it satisfy  $\gamma_{10} = \gamma_{01}$ , corresponding in this case for emission and absorption of a quanta  $\Delta\epsilon_w = \epsilon_1$  from the work source.

### III. THERMODYNAMIC PERFORMANCE

We are interested in the performance of the quantum thermal machine models presented in the previous section when operating in non-equilibrium steady-state conditions [1, 15]. By performance, we refer not only to the size of the output current generated by the machine operation (output power in the case of heat engines or cooling power for the case of refrigerators) and the machine thermodynamic efficiency (ratio of useful output to source input), but also to the size of the fluctuations in the output current, which can be viewed as measure of the “quality” of that output in stochastic machines [27].

Under steady-state conditions,  $\mathcal{L}(\pi) = 0$ , the average output power generated by the machine on the external drive and the average heat current absorbed from reservoir  $r$ , are given, respectively, by standard definitions [70]:

$$\langle \dot{W} \rangle := -\text{Tr}[\dot{H}(t)\pi(t)] = -\text{Tr}[\dot{V}(t)\pi(t)], \quad (12)$$

$$\langle \dot{Q}_r \rangle := \sum_k \text{Tr}[H_0 \mathcal{D}_k^{(r)}[\pi(t)]], \quad (13)$$

where we recall that  $\pi(t)$  may acquire a periodic time-dependence (in Schrödinger picture) due to the presence

of non-diagonal elements (coherences) in the steady-state density operator. We also emphasize that for weak perturbations as the ones considered here, only the bare Hamiltonian  $H_0$  enters in the heat currents [71, 72], ensuring consistency with the second law [73]. The first law takes the form  $\langle \dot{W} \rangle = \sum_r \langle \dot{Q}_r \rangle$ , imposing that any output power is sustained by input heat currents from the baths. Explicit expressions of the heat currents  $\langle \dot{Q}_r \rangle$  valid for generic machines (with or without degeneracy) are given in Appendix A.

As a consequence of Markovianity, the second law in the setup is manifested through the non-negativity of the entropy production rate:

$$\langle \dot{S}_{\text{tot}} \rangle = -\sum_r \beta_r \langle \dot{Q}_r \rangle \geq 0, \quad (14)$$

which characterizes the irreversibility of the machine operation in its nonequilibrium steady-state [2, 71]. Here it is also worth remarking that whenever the temperature of some of the reservoirs  $r$  approaches infinity,  $\beta_r \rightarrow 0$ , the associated energy current does not contribute to the entropy production and hence it should be considered as (incoherent) work rather than heat, see also Refs. [7, 74]. In that case the output power associated to such a work reservoir reads  $\langle \dot{W} \rangle = -\sum_k \text{Tr}[H_0 \mathcal{D}_k^{(r)}[\pi(t)]]$ .

The efficiency of thermal machines can be defined from the ratio of the average output useful current to the average input resource one, as determined by the operational mode of the machine:

$$\eta := \frac{\langle J_{\text{out}} \rangle}{\langle J_{\text{in}} \rangle}, \quad (15)$$

where in the case of heat engine operation  $J_{\text{out}} = \langle \dot{W} \rangle$  and  $J_{\text{in}} = \langle \dot{Q}_h \rangle$ , while for refrigeration the efficiency (coefficient of performance) is given from  $J_{\text{out}} = \langle \dot{Q}_c \rangle$  and either  $J_{\text{in}} = -\langle \dot{W} \rangle$  for power-driven refrigerators (as the models in Secs. II A and II C), or  $J_{\text{in}} = -\langle \dot{Q}_h \rangle$  for absorption refrigerators (as the one in Sec. II B). For extensions of efficiency to multiple inputs and outputs see e.g. Refs. [75–77].

By combining the first and second laws in the setup we recover Carnot bound for the efficiency of heat engines  $\eta \leq \eta_C := 1 - \beta_h/\beta_c$ , as well as the corresponding (Carnot) bounds for power-driven fridges  $\eta \leq \eta_{\text{fr}} := \beta_h/(\beta_c - \beta_h)$  and absorption refrigerators,  $\eta \leq \eta_{\text{abs}} := (\beta_m - \beta_h)/(\beta_c - \beta_m)$ , achieved in the limit of zero entropy production, where all energy currents vanish [1, 15, 50].

The maximum efficiency (zero power) equilibrium points separate the different modes of operation of the machines, where heat currents and output power change sign. In the models presented here they can be easily obtained analytically by noticing that the average steady-state currents can be rewritten as:

$$\langle \dot{Q}_r \rangle = \Delta\epsilon_r \langle \dot{N}_r \rangle, \quad (16)$$

where  $\langle \dot{N}_r \rangle$  is the probability current associated to the reservoir  $r$  (flux of quanta). It results from the fact that

	Heat engine/pump	Refrigerator
Three-level amplifier	$\omega_d/\epsilon_2 \leq \eta_C$	$\eta_C \leq \omega_d/\epsilon_2 \leq 1$
Autonomous fridge	$\eta_{\text{abs}} \leq \epsilon_1/\epsilon_3 \leq 1$	$\epsilon_1/\epsilon_3 \leq \eta_{\text{abs}}$
NIC machine	$\epsilon_1/\epsilon_2 \leq \eta_C$	$\eta_C \leq \epsilon_1/\epsilon_2 \leq 1$

TABLE I. Parameter relations leading to the main modes of operation of the three thermal machines examined here. In the case of the autonomous (absorption) refrigerator the heat engine regime is replaced by heat pumping.

in the models baths are associated to a single energy gap  $\Delta\epsilon_r$ . In the steady state, due to the absence of leaks, the system will exchange excitations with all baths at the same rate, i.e.  $\forall i, j$  we have  $\langle \dot{N}_i \rangle = \langle \dot{N}_j \rangle := \langle \dot{N} \rangle$ . In addition, the first law constrains the average value of the work to satisfy  $\langle \dot{W} \rangle = \sum_r \Delta\epsilon_r \langle \dot{N} \rangle = \omega_d \langle \dot{N} \rangle$ . The ratio between the different steady-state currents hence verify

$$\frac{|\langle \dot{W} \rangle|}{|\langle \dot{Q}_j \rangle|} = \frac{\omega_d}{\epsilon_j} \quad ; \quad \frac{|\langle \dot{Q}_i \rangle|}{|\langle \dot{Q}_j \rangle|} = \frac{\epsilon_i}{\epsilon_j}. \quad (17)$$

By combining the above proportionality relations with the efficiency bounds above we can construct a table for the operational modes of each model (see Table I).

While it is in general desirable for any thermal machine to have a large output current and a high efficiency (low rate of entropy production), in microscopic systems another fundamental factor to consider is the fluctuations associated with the currents, specially in the output power. Therefore, in addition to minimizing entropy production and maximizing power, low fluctuations (resulting in higher precision) in energy flows are also desirable. In classical systems these three quantities are not independent, but their trade-off is quantified by the TUR:

$$\mathcal{Q} = \langle \dot{S}_{\text{tot}} \rangle \frac{\text{Var}[J_{\text{out}}]}{\langle J_{\text{out}} \rangle^2} \geq 2, \quad (18)$$

where  $\langle J_{\text{out}} \rangle$  and  $\text{Var}[J_{\text{out}}]$  denote the mean and variance of the useful output current i.e  $J_{\text{out}} = \dot{W}, \dot{Q}_c$  for work production and refrigerator regimes respectively. Initially proposed in the context of bio-molecular processes [24], the TUR was then formally established in stochastic thermodynamics [25, 26], and subsequently applied to classical steady-state heat engines [27], for which the TUR ratio  $\mathcal{Q}$  in Eq. (18) can be rewritten in terms of the output power and efficiency as:

$$\mathcal{Q}_{\text{he}} = \beta_c \frac{\text{Var}[\dot{W}]}{\langle \dot{W} \rangle} \left( \frac{\eta_C - \eta}{\eta} \right), \quad (19)$$

where we identified  $J_{\text{out}} = \dot{W}$  and  $\langle \dot{S}_{\text{tot}} \rangle = -\beta_h \langle \dot{Q}_h \rangle - \beta_c \langle \dot{Q}_c \rangle = \beta_c (\eta_C/\eta - 1) \langle \dot{W} \rangle$ . Analogously by taking  $J_{\text{out}} = \dot{Q}_c$  and rewriting the expression for the entropy production rate, we obtain the corresponding TUR ratio for power-driven refrigerators:

$$\mathcal{Q}_{\text{fr}} = (\beta_c - \beta_h) \frac{\text{Var}[\dot{Q}_c]}{\langle \dot{Q}_c \rangle} \left( \frac{\eta_{\text{fr}} - \eta}{\eta} \right). \quad (20)$$

Finally, for the case of absorption refrigerators we obtain the TUR ratio:

$$\mathcal{Q}_{\text{abs}} = (\beta_c - \beta_m) \frac{\text{Var}[\dot{Q}_c]}{\langle \dot{Q}_c \rangle} \left( \frac{\eta_{\text{abs}} - \eta}{\eta} \right), \quad (21)$$

where in this case we identified  $J_{\text{out}} = \dot{Q}_c$  and the entropy production rate reads  $\langle \dot{S}_{\text{tot}} \rangle = -\beta_h \langle \dot{Q}_h \rangle - \beta_c \langle \dot{Q}_c \rangle - \beta_m \langle \dot{Q}_m \rangle = (\beta_c - \beta_m) (\eta_{\text{abs}}/\eta - 1) \langle \dot{Q}_c \rangle$ . Throughout this paper, to evaluate fluctuations in the output currents, i.e. the variances  $\text{Var}[\dot{W}]$  and  $\text{Var}[\dot{Q}_c]$ , we employ the full-counting statistics (FCS) formalism [78, 79] (see details in Appendix B).

In any of the three cases, the TUR implies that beyond a certain threshold, a classical Markovian engine can only enhance its precision in the output (cooling) power at the cost of either reducing the output itself or reducing the energy efficiency, so that the above ratio remains bounded by 2, i.e.  $\mathcal{Q} \geq 2$ . However, some models of quantum thermal machines have been shown to produce violations of the TUR, that is, they verify  $\mathcal{Q} < 2$  (see e.g. Refs. [28–33]). Such violations act as a witness indicating an enhanced tradeoff between power, precision and efficiency that arise in certain parameter regimes. Nevertheless, it is in principle unclear whether that violations may occur in relevant regimes, i.e. where the machine performs in an optimal way, providing a practical quantum-thermodynamic advantage. In addition, such quantum-thermodynamic advantages may arise even if the TUR is not violated, since classical machines may not saturate the TUR in such relevant regimes. Hence in order to provide a fair and accurate assessment of practical quantum-thermodynamic advantages in thermal machines both optimization of the machine performance and comparison to classical models become necessary.

#### IV. CLASSICAL-THERMODYNAMIC EQUIVALENTS OF THERMAL MACHINES

Throughout this paper, inspired by the notion of classical emulability introduced in Ref. [23], we use the term “classical-thermodynamic equivalent” (or simply “classical equivalent”) of a quantum thermal machine to refer to a thermal machine model with same bare Hamiltonian,  $H_0$ , but whose evolution can be described using only classical (Markovian) dynamics, while being capable of producing the same average currents as the quantum machine using the same amount of incoherent resources. Notice that if the classical equivalent machine is capable of producing the same average currents, this also ensures the same efficiency as the original quantum machine. However, quantum and classical equivalent models may differ in general in their fluctuations.

By using same incoherent resources we mean that the classical-thermodynamic equivalent model is in contact with the same thermal baths, and therefore have access to the same temperatures. Furthermore the requisite of

having same bare Hamiltonian implies that the classical equivalent also has the same energy level structure as the original quantum machine, which allow us to identify them as the “same machine”. This is in contrast with other notions of classical analogs in thermal machines where all the parameters of the classical model are imposed to be exactly equal, including the couplings to the baths or the driving strength [9, 12] (this is also the case of introducing extra dephasing in the quantum model). Here instead we allow to vary these parameters as long as the requirements for weak-coupling and Markovian dynamics assumed for the thermal machine models are satisfied. This choice is not arbitrary, but allows for a stringer notion of quantum-thermodynamic advantage that avoids spurious “advantages” that may disappear by just slightly modifying some of the parameters in the model.

In the following, we develop a general method for constructing these equivalent machines in situations where the coherence in the system arises either from Hamiltonian dynamics (Hamiltonian-induced coherence) or from dissipative processes (noise-induced coherence).

### A. Hamiltonian-induced coherence

Since we want the classical equivalent to produce the same average energy currents than the quantum counterpart, our starting point will be the generic expression for the heat currents given in Eq. (13). This expression, valid for any given (bare) Hamiltonian  $H_0$ , can be rewritten as (see App. A):

$$\langle \dot{Q}_r \rangle = \sum_{i < j}^{\in B_r} (\epsilon_j - \epsilon_i) (\gamma_{ij} \pi_{ii} - \gamma_{ji} \pi_{jj}), \quad (22)$$

where we remind the reader that transitions in the sum above are restricted to the ones induced in the set  $B_r$ , i.e. induced by reservoir  $r$ . The above expression only depends on the level populations (diagonal elements of the density matrix), energy gaps of the machine and jump rates. As a consequence, the useful output current of the machine can only depend on these quantities as follows from the first law, e.g. in heat engines  $\langle \dot{W} \rangle = \sum_r \langle \dot{Q}_r \rangle$ . Given that the energy gaps and temperatures of the reservoirs are fixed, we conclude that to ensure identical input and output currents, the quantum machine and its classical equivalent must have matching diagonal elements in their steady-state density matrices.

In order to mimic the same level populations in the classical equivalent, we proceed by first solving the equations of motion for the diagonal elements and non-vanishing coherences in the quantum machine (details of this procedure are presented in Appendix C). Let's denote by indices  $|u\rangle$  and  $|v\rangle$  a couple of levels that are connected by  $V$  (for simplicity we assume  $|u\rangle$  and  $|v\rangle$  not further connected to other levels). The equations of

motion for these two levels read:

$$\begin{aligned} \dot{\rho}_{uu} &= \sum_{j \neq u} \gamma_{ju} \rho_{jj} - \rho_{uu} \sum_i \gamma_{ui} - 2g \text{Im}(\rho_{uv}), \\ \dot{\rho}_{vv} &= \sum_{j \neq v} \gamma_{jv} \rho_{jj} - \rho_{vv} \sum_i \gamma_{vi} + 2g \text{Im}(\rho_{uv}), \\ \dot{\rho}_{uv} &= -\frac{1}{2} \sum_i (\gamma_{ui} + \gamma_{vi}) \rho_{uv} - ig(\rho_{vv} - \rho_{uu}), \end{aligned} \quad (23)$$

while for the rest of levels  $n \neq \{u, v\}$ , not connected by  $V$ , we simply have  $\dot{\rho}_{nn} = \sum_{j \neq n} \gamma_{jn} \rho_{jj} - \rho_{nn} \sum_i \gamma_{ni}$ .

Following Ref. [23], by equating all the derivatives to zero in Eqs. (23), we can determine the relation between the coherence of levels connected by the Hamiltonian  $V$  and their populations (that should be verified in the steady state):

$$\pi_{uv} = \frac{-2ig(\pi_{vv} - \pi_{uu})}{\sum_i (\gamma_{ui} + \gamma_{vi})}. \quad (24)$$

Then we introduce the above dependence back into off-diagonal elements in Eqs. (23), to obtain that the net effect of coherence in the steady state is equivalent to adding a virtual transition promoting jumps between the interacting levels  $|u\rangle$  and  $|v\rangle$ :

$$\begin{aligned} \frac{d}{dt} \rho_{uu} &= \sum_{j \neq u} \gamma_{ju} \rho_{jj} - \rho_{uu} \sum_i \gamma_{ui} + \gamma_{vu}^{\text{cl}} \rho_{vv} - \gamma_{uv}^{\text{cl}} \rho_{uu}, \\ \frac{d}{dt} \rho_{vv} &= \sum_{j \neq v} \gamma_{jv} \rho_{jj} - \rho_{vv} \sum_i \gamma_{vi} + \gamma_{uv}^{\text{cl}} \rho_{uu} - \gamma_{vu}^{\text{cl}} \rho_{vv}, \end{aligned} \quad (25)$$

with transition rate

$$\gamma_{uv}^{\text{cl}} = \gamma_{vu}^{\text{cl}} = \frac{4g^2}{\sum_i (\gamma_{ui} + \gamma_{vi})}. \quad (26)$$

As a consequence, if we replace the Hamiltonian term  $V$  responsible for the coherent interaction between levels  $|u\rangle$  and  $|v\rangle$  by the above extra stochastic transition between them, the system governed by Eqs. (25) will reach a steady-state with exactly the same populations as the original one governed by Eq. (23), and therefore the same currents in Eq. (22).

We have thus achieved a classical equivalent of the quantum model in which the dynamics is entirely classical, as given by a set of incoherent jumps between the machine energy levels, while reproducing the same (average) currents in the steady state. We also notice that the equivalent machine is coupled to the same set of thermal baths, while the coherent interaction is replaced by an stochastic jump process without bias in either direction. This provides a classical equivalent model that uses the same amount of incoherent resources. In the case of energetic coherence, i.e. non-degenerate levels  $|u\rangle$  and  $|v\rangle$  ( $\epsilon_u \neq \epsilon_v$ ) this means replacing the quantum-coherent work source (battery) by a classical stochastic

work source (battery), like a bath at infinite temperature. On the other hand, in the case of degenerate coherence ( $\epsilon_u = \epsilon_v$ ) the extra stochastic transition is a source of pure noise without any associated energy current and can hence be considered as free.

## B. Noise-induced coherence

In this case, we find that the heat currents of the collective transitions explicitly depend on the real part of the coherence between energy levels involved in the environmental noise-inducing mechanism (which we again denote  $|u\rangle$  and  $|v\rangle$ ):

$$\begin{aligned} \langle \dot{Q}_r \rangle &= \sum_{i < j} (\epsilon_j - \epsilon_i) (\gamma_{ij} \pi_{ii} - \gamma_{ji} \pi_{jj}) \\ &+ 2 \sum_j (\epsilon_j - \epsilon_v) (\gamma_{uj} + \gamma_{vj}) \text{Re}(\pi_{uv}), \end{aligned} \quad (27)$$

while the currents that are not involved in the noise-inducing mechanism are given by Eq. (22) as in the previous case (see App. A). Moreover, in Appendix C we show that reproducing the steady-state populations results again in equal average currents, despite of the appearance of the second contribution in Eq. (27).

Following the same procedure as for Hamiltonian-induced coherence, we can observe the net effect of coherence in the steady state by solving the equations of motion and replacing the dependence of coherence back into the equations (see details in App. C):

$$\pi_{uv} = \frac{\sum_i [2\sqrt{\gamma_{ui}\gamma_{vi}}\pi_{ii} - \sqrt{\gamma_{iu}\gamma_{iv}}(\pi_{uu} + \pi_{vv})]}{\sum_i (\gamma_{iu} + \gamma_{iv})}. \quad (28)$$

As before, we obtain a virtual jump between the coherent levels  $u$  and  $v$ , but in this case we also find corrections to the rates in some of the (already present) jumps involving these levels and other levels of the machine  $n$ . Thus the rates for the classical equivalent must be of the form:

$$\begin{aligned} \gamma_{uv}^{\text{cl}} &= \gamma_{vu}^{\text{cl}} = \frac{\left(\sum_j \sqrt{\gamma_{uj}\gamma_{vj}}\right)^2}{\sum_j (\gamma_{uj} + \gamma_{vj})}, \\ \gamma_{in}^{\text{cl}} &= \gamma_{in} - 2\sqrt{\gamma_{un}\gamma_{vn}} \gamma_{uv}^*, \\ \gamma_{ni}^{\text{cl}} &= \gamma_{ni} - 2\sqrt{\gamma_{nu}\gamma_{nv}} \gamma_{uv}^*, \end{aligned} \quad (29)$$

where  $i = u, v$  above and we defined  $\gamma_{uv}^* := \frac{\sum_j \sqrt{\gamma_{uj}\gamma_{vj}}}{\sum_j (\gamma_{uj} + \gamma_{vj})}$ . It can be proved that local detailed balance relations are not modified in any transition of the machine by the corrections to the rates above. To show this, let us rewrite the rates of the collective transitions to and from levels  $i = \{u, v\}$  as  $\gamma_{in} = \gamma_r^i \exp[\beta_r(\epsilon_i - \epsilon_n)/2]$  and  $\gamma_{ni} = \gamma_r^i \exp[-\beta_r(\epsilon_i - \epsilon_n)/2]$  respectively, where  $\gamma_r^i := \sqrt{\gamma_{in}\gamma_{ni}}$  is a purely kinetic (spontaneous-emission-like) contribution to the rates not depending on the direction of the jumps, and  $\beta_r$  is the

temperature of the bath to which the transition is coupled. Using this notation the corrected rates read

$$\begin{aligned} \gamma_{in}^{\text{cl}} &= \left(\gamma_r^i - 2\gamma_{uv}^* \sqrt{\gamma_r^u \gamma_r^v}\right) \exp[\beta_r(\epsilon_i - \epsilon_n)/2], \\ \gamma_{ni}^{\text{cl}} &= \left(\gamma_r^i - 2\gamma_{uv}^* \sqrt{\gamma_r^u \gamma_r^v}\right) \exp[-\beta_r(\epsilon_i - \epsilon_n)/2]. \end{aligned} \quad (30)$$

Notice that the corrections only affect the purely kinetic contributions to the rates, but not their bias. As a consequence, the classical equivalent will employ the same thermodynamic resources (temperatures and energy gaps) as the quantum system. In other words, in order to construct the classical equivalent machine we can replace the collective transitions appearing in the original quantum model by local ones (with a tuned rate) to the same thermal baths, and add an extra stochastic transition between the degenerated levels  $|u\rangle$  and  $|v\rangle$ .

## V. THERMODYNAMIC IMPACT OF COHERENCE

We are now in a position to present our results that unveil the impact of steady-state coherence in the performance of quantum thermal machines by direct comparison with the corresponding classical equivalents as introduced above. We recall that, by construction, the classical equivalent machine reproduces the same average currents in all the transitions, and hence it has the same efficiency than the original machine. However, fluctuations in the output current (as captured by the variance), can differ in general between quantum and classical models, making the presence of coherence either beneficial or detrimental for the machine output reliability. In the following, we show that energetic coherence can lead to reliability improvements (for same output and efficiency), while, on the contrary, thermal machines operating with degenerate coherence can only perform equal or worst than their classical-equivalent counterparts.

In order to address the impact of coherence in the reliability of the thermal machines, we introduce the fluctuations ratio  $\mathcal{R}$  between quantum and classical machines as

$$\mathcal{R} := \frac{\text{Var}[J_{\text{out}}]}{\text{Var}[J_{\text{out}}^{\text{cl}}]}, \quad (31)$$

where  $J_{\text{out}}^{\text{cl}}$  denotes the output current in the classical-equivalent model. The above ratio measures the relative reduction in the dispersion of the output current in the quantum machine, as compared to the classical one. If  $\mathcal{R} > 1$ , then the classical equivalent provides a more accurate output;  $\mathcal{R} = 1$  implies that the quantum and classical models are indistinguishable from their dispersion, and  $\mathcal{R} < 1$  implies that the output in the quantum machine is more accurate, hence providing a quantum-thermodynamic advantage manifested in an enhanced reliability of the machine for same average outputs.

Our analysis is performed as follows: we first obtain the classical equivalents for the three prototypical machines considered here as explained in Sec. IV. Then we



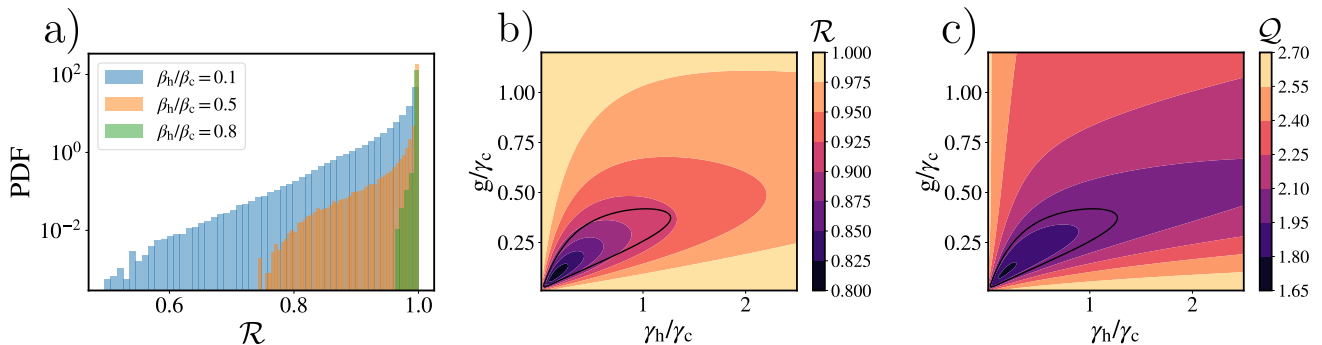


FIG. 2. a) Histogram of sampled values of the ratio between the fluctuations of the system and its classical analog  $\mathcal{R}$  for different ratios of the bath temperatures (see legend). The values corresponds to an exploration of the following region in the parameters space of the system:  $\beta_c = 1$ ,  $\epsilon_2 = 5$ ,  $\omega_d \in [0.1, 4.9]$ ,  $\gamma_{h/c} \in [10^{-5}, 10^{-2}]$  and  $g \in [10^{-5}, 10^{-2}]$ . b) Colour maps of the fluctuation ratio  $\mathcal{R}$  and c) the TUR ratio  $\mathcal{Q}_{\text{he}}$  as a function of the bath interaction strengths and the driving force. The other systems parameters are:  $\beta_c = 1$ ,  $\beta_h = 0.1$ ,  $\epsilon_2 = 5$ ,  $\omega_d = 2.5$  and  $\gamma_c = 10^{-3}$ .

obtain, using the FCS approach, the variance of the output currents for both quantum and classical equivalent models (details are provided in App. B). Finally, we numerically generate a  $10^6$  number of possible system configurations in the whole parameters space verifying the basic assumptions ensuring the consistency of the Markovian dynamics and conduct a direct comparative analysis.

### A. Thermodynamic enhancement through energetic coherence

We provide evidence that in thermal machines that show steady-state energetic coherence (as the one induced by a weak external coherent driving) quantum-thermodynamic improvements can be achieved in the form of reduced fluctuations in the output current for given (fixed) power output and efficiency. As a paradigmatic example, we use the three-level amplifier (see Fig. 1a) as introduced in Sec. II A, to illustrate this point.

Following the general recipe provided in Sec. IV, the classical equivalent of the three-level amplifier can be obtained by replacing the driving Hamiltonian  $V(t)$  by an extra stochastic transition between levels  $|0\rangle$  and  $|1\rangle$ . The rates of these extra transitions, as given by Eq. (26) become  $\gamma_{01}^{\text{cl}} = \gamma_{10}^{\text{cl}} = 4g^2/(\gamma_h \bar{n}_h + \gamma_c \bar{n}_c)$ .

In order to quantify the impact of (energetic) coherence in the three-level amplifier, we compute the fluctuations ratio  $\mathcal{R}$  in Eq. (31) for the output power,  $J = \dot{W}$ . Exploring the model parameters for fixed external temperatures of the baths, we observe the appearance of a significant amount of configurations with  $\mathcal{R} < 1$ , that increases as the temperature bias powering the machine increases. This is illustrated in Fig. 2a where the distribution of  $\mathcal{R}$  values over  $10^6$  configurations is shown for three different choices of (fixed) environmental temperatures. As can be appreciated, for all configurations we obtain  $\mathcal{R} \leq 1$ , that is, the three-level amplifier always match or exceed

the performance of the corresponding classical equivalent machine for each configuration, hence unveiling a beneficial role of energetic coherence. Improvements reaching an output power variance reduction up to  $\mathcal{R} \sim 1/2$  are possible for temperature bias of the order  $T_h = 10T_c$ . We also observe a fat tail in the distribution that ensures the robustness of the enhancements, meaning that many configurations can lead to significant reductions in the output variance. The range of variance reductions shrinks towards higher  $\mathcal{R}$  values as the temperature bias is reduced, and tends to disappear close to equilibrium (similar temperatures of the baths) where quantum and classical models perform almost equally. This effect is a manifestation of the nonequilibrium character of the enhancements produced by energetic coherence.

In Fig. 2b the behaviour of the fluctuations reduction ratio,  $\mathcal{R}$  in Eq. (31), is plotted as a function of the spontaneous emission rates and the driving strength. Darker colours denote regions where larger stability enhancements with respect to the classical equivalent machine are obtained, which are verified in the regime of very weak driving and highly asymmetric spontaneous rates (low coupling strength with the hot bath as compared to the cold one). This plot can be contrasted with Fig. 2c where the TUR ratio in Eq. (19) is shown for the same range of parameters. In both plots the black solid line has been introduced as a guide to the eye representing the boundary ( $\mathcal{Q}_{\text{he}} = 2$ ) of the region where TUR violations are obtained. This allows the comparison of the method using the classical equivalent machine to detect quantum-thermodynamic enhancements, with the direct search for violations of the (classical) TUR [28–33].

We observe that the area where violations of the TUR,  $\mathcal{Q}_{\text{he}} < 2$ , are verified, is contained within the region  $\mathcal{R} < 1$  and indeed coincide with the highest improvements in precision as measured by the reduction ratio  $\mathcal{R}$ . However, as expected, we also find that even in regimes where the TUR is not violated, there exists an improvement in accuracy of the output current due to the pres-

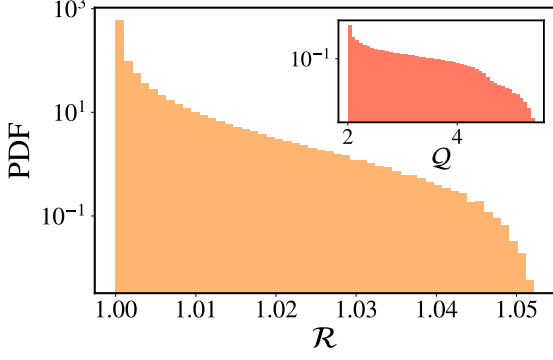


FIG. 3. Histogram of sampled values of  $\mathcal{Q}$  (inset plots) and the ratio between the fluctuations of the system and its classical equivalent  $\mathcal{R}$  (outset plots). The values corresponds to an exploration of the following region in the parameters space of the system:  $\beta_c = 1$ ,  $\beta_m/\beta_c \in [0, 1]$ ,  $\beta_h/\beta_m \in [0, 1]$ ,  $\epsilon_2 = 5$ ,  $\epsilon_1 \in [0.1, 4.9]$ ,  $\gamma_{c/m/h} \in [10^{-5}, 10^{-2}]$  and  $g \in [10^{-4}, 10^{-2}]$ .

ence of energetic coherence. Therefore, using the classical equivalent of the original three level amplifier, we are able to identify regimes of thermodynamic enhancement that cannot be revealed by violations of the TUR.

### B. Thermodynamic disadvantage caused by degenerate coherence

We now use the same methodology to carry out a similar analysis for the cases of degenerate (non-energetic) coherence, taking as main examples the three-qubit autonomous refrigerator introduced in Sec. II B and the NIC machine model introduced in Sec. III C.

Starting with the autonomous refrigerator, we find that the classical equivalent is obtained by replacing the three-body interaction Hamiltonian  $V$  allowing the exchange of energy between qubits, by a classical transition producing incoherent jumps between levels  $|101\rangle$  and  $|010\rangle$ . The rate of this transition, according to Eq. (26) becomes in this case  $\gamma_{uv}^{cl} = \gamma_{vu}^{cl} = 4g^2/\sum_r (2\bar{n}_r + 1)\gamma_r$ , where  $|u\rangle = |101\rangle$  and  $|v\rangle = |010\rangle$ , and the sum runs over the three baths,  $r = h, m, c$ .

For assessing the enhancements in the reliability of the refrigerator, the fluctuations ratio  $\mathcal{R}$  in Eq. (31) is computed for the cooling power (heat current from the cold bath),  $J_{out} = \dot{Q}_c$ . The distributions for the reduction ratio  $\mathcal{R}$  and TUR ratio  $\mathcal{Q}_{abs}$  (inset) in this case are shown in Fig. 3 again for  $10^6$  parameter configurations. As can be observed, in this case we obtain  $\mathcal{R} \geq 1$  for all configurations, meaning that a reduction of the fluctuations ratio is not possible. As a consequence, we have to conclude that the three-qubit quantum refrigerator does not perform better than its classical equivalent, despite it has been shown to operate using entanglement [20]. In particular, in the majority of cases, the fluctuations in both systems are comparable, with certain cases where

the quantum system exhibits noise levels up to 5% higher than its classical thermodynamic equivalent. Looking at the distribution of  $\mathcal{Q}_{abs}$  values, we also see that the autonomous refrigerator remains unable to break the classical constraint imposed by the TUR in all system configurations (inset plot). Consequently, we conclude that degenerate coherence does not have a significant impact on the autonomous refrigerator performance, which is not able to beat its classical equivalent counterpart in all the parameter regions.

In the case of the NIC machine, previous studies have shown that when the rates of the collective transitions were equal ( $\gamma_{na} = \gamma_{nb}$  and  $\gamma_{an} = \gamma_{bn}$  for  $n = 0, 1$ ) it is possible to apply a change of variables that effectively decouples coherences from populations [66] (see also Ref. [71] for a similar case). However, such change of variables does not produce this decoupling when the rates are unequal, suggesting that the system enters a purely quantum regime [69]. In the following, we show that in both cases a classical equivalent can be defined for large regions of the parameter space, that can be used to evaluate the thermodynamic impact of noise-induced coherence.

We first introduce the following basis change where the degenerate levels  $|2a\rangle$  and  $|2b\rangle$  are transformed into levels  $|\alpha\rangle$  and  $|\beta\rangle$ :

$$\begin{aligned} |\alpha\rangle &= \frac{1}{\sqrt{\gamma_h^a + \gamma_h^b}} \left( \sqrt{\gamma_h^a} |a\rangle + \sqrt{\gamma_h^b} |b\rangle \right), \\ |\beta\rangle &= \frac{1}{\sqrt{\gamma_h^a + \gamma_h^b}} \left( \sqrt{\gamma_h^b} |a\rangle - \sqrt{\gamma_h^a} |b\rangle \right). \end{aligned} \quad (32)$$

Notice that in the case of symmetric rates for the hot reservoir,  $\gamma_h^a = \gamma_h^b$ , this expression becomes the one presented in Ref. [69], but differs otherwise. By introducing this change, we successfully decouple the state  $|\beta\rangle$  from the state  $|0\rangle$ , resulting in a machine with only one explicit collective transition, as illustrated in Fig. 4a. For symmetric rates, we recover the situation where  $|\beta\rangle$  is completely decoupled from the states  $|0\rangle$  and  $|1\rangle$ , leading to a classical three-level system with local jumps at same temperatures than the original NIC machine.

In the general case, following Sec. IV B, the classical equivalent includes an extra stochastic transition between the degenerate levels reading:

$$\gamma_{\alpha\beta}^{cl} = \gamma_{\beta\alpha}^{cl} = \frac{(\bar{n}_h + 1)\gamma_h^\alpha\gamma_h^\beta}{(\bar{n}_c + 1)\gamma_c^\alpha + (\bar{n}_h + 1)(\gamma_h^\alpha + \gamma_h^\beta)}, \quad (33)$$

and corrections to the rates of the collective transitions between the degenerate levels and the other ones as

$$\begin{aligned} \gamma_{k1}^{cl} &= (\gamma_h^k - 2\gamma_{\alpha\beta}^{cl})(\bar{n}_h + 1), \\ \gamma_{1k}^{cl} &= (\gamma_h^k - 2\gamma_{\alpha\beta}^{cl})\bar{n}_h, \end{aligned} \quad (34)$$

for  $k = \alpha, \beta$ . By examining the above equations, we find that the corrections to the spontaneous emission

rates can make these rates eventually negative, which would correspond to a nonphysical situation. Consequently, the construction of the classical equivalent for noise-induced coherence is limited to scenarios that ensure positive rates. For the NIC machine analyzed here, this happens when

$$\gamma_h^\alpha + \gamma_h^\beta \geq 2\max[\gamma_h^\alpha, \gamma_h^\beta] - \frac{\bar{n}_c + 1}{\bar{n}_h + 1}\gamma_c^\alpha, \quad (35)$$

as illustrated in Fig. 4b.

We compute the fluctuation ratio  $\mathcal{R}$  in Eq. (31) for the NIC machine and its classical equivalent by taking again  $J_{\text{out}} = \dot{W}$  for  $10^6$  different parameter configurations within the region where the classical equivalent machine can be defined. In Fig. 5 we show the distribution of  $\mathcal{R}$  together with the corresponding distribution of the TUR ratio  $\mathcal{Q}_{\text{he}}$  values (see inset). Our results show that  $\mathcal{R} \geq 1$  for all cases, similarly to the case of the autonomous refrigerator. In particular, we find that the quantum-coherent machine is at least as noisy (or more) than its classical equivalent. Indeed for some configurations the NIC machine reaches noise levels up to 30% higher than its classical counterpart. By looking at the inset we observe that, as expected, the TUR is also not violated for all choices of parameters ( $\mathcal{Q}_{\text{he}} \geq 2$  always) in accordance to previous studies about TUR violations in similar models [68].

Therefore it becomes clear that the NIC machine is not able to overcome the classical equivalent machine in any of the relevant configurations. Our results hence imply that noise-induced coherence has not any beneficial impact in the thermodynamic performance of the NIC machine, whose operation in terms of power, efficiency and reliability can be mimicked (or surpassed) by a purely classical equivalent machine using the same set of resources. These conclusions are in contrast with previous claims in the literature regarding quantum enhancements in NIC models, see e.g. Refs. [16–19], which either lacked a systematic comparison to classical equivalent models, or were judged on the basis of more limiting notions of

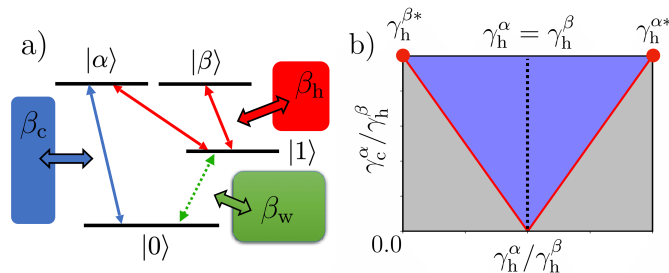


FIG. 4. (a.) Schematic representation of the level transitions in the Noise-induced machine after the variable change. (b.) Graphical representation of the inequality (35) separating the regimes where we can define the classical equivalent for noise-induced coherence (blue zone) and where we cannot (grey zone).

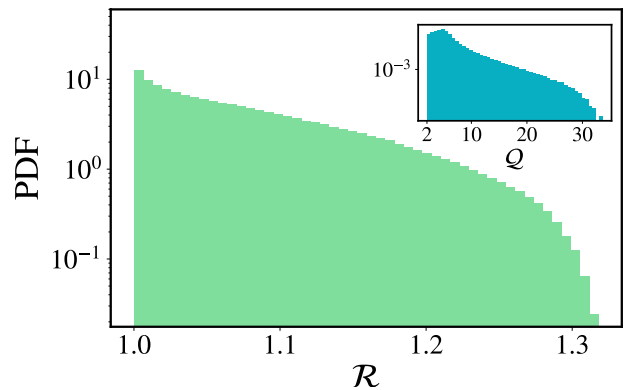


FIG. 5. Histogram of sampled values of  $\mathcal{Q}$  (inset plots) and the ratio between the fluctuations of the system and its classical equivalent  $R$  (outset plots). The values corresponds to an exploration of the following region in the parameters space of the system:  $\beta_w \rightarrow \infty$ ,  $\beta_c = 1$ ,  $\beta_h/\beta_c \in [0, 1]$ ,  $\epsilon_2 = 5$ ,  $\epsilon_1 \in [0.1, 4.9]$ ,  $\gamma_h^{(a/b)} \in [10^{-5}, 10^{-2}]$  and  $\gamma_c^{(a/b)} = 10^{-3}$ .

classical equivalent (e.g. requiring all model parameters to be maintained equal).

## VI. PARETO OPTIMIZATION AND PRACTICAL ADVANTAGES

In the previous section we have seen that only for the case of energetic coherence, corresponding to the case of the three-level amplifier introduced in Sec. II A, a quantum-thermodynamic advantage can be identified for different set of parameters in the model. The reduction of the output current fluctuations as compared to classical equivalent machines operating at same (average) output power and efficiency, provide indeed necessary conditions for a quantum-thermodynamic advantage. Still in order to proof a practical (and hence useful) advantage, an analysis of the regimes where such an improved reliability is obtained is needed. Here we show that the advantages identified before occur indeed along optimal performance, e.g. for maximum power and for maximum efficiency regimes.

Since optimizing the machine performance involves more than one desired objective (maximize power, maximize efficiency, minimize fluctuations), multi-objective optimization techniques, also called Pareto optimization, are required. These techniques are well known in engineering [80] and have been applied to a wide range of problems, from network theory [34] to betting strategies [35] and phenotypic response [36]. They have also attracted some attention recently in the field of stochastic and quantum thermodynamics, where they have been applied to the optimisation of heat engine cycles in the slow-driving regime [37–39].

In order to solve a multi-objective optimisation problem (let's take for example a two-dimensional problem)

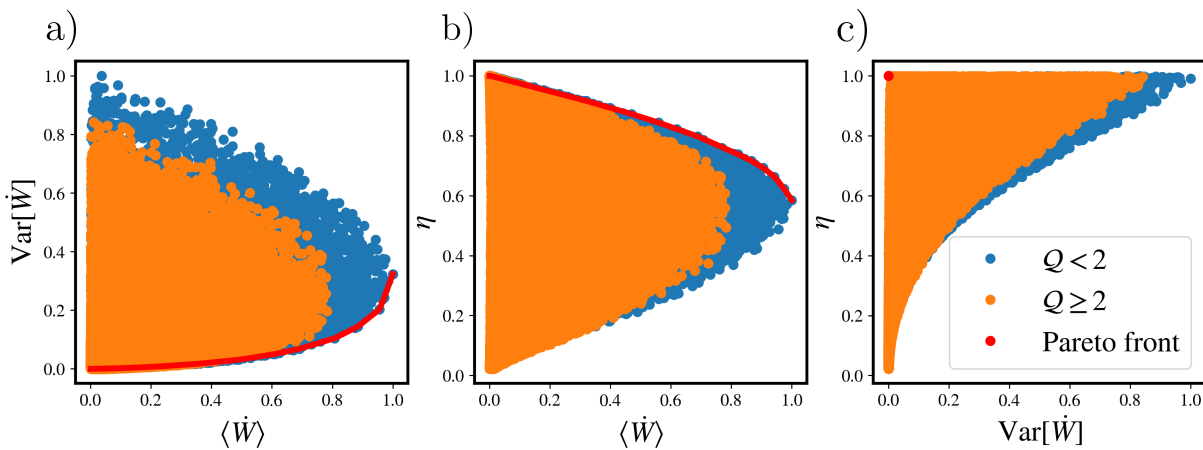


FIG. 6. Two dimensional multi-objective optimization of the different thermodynamic quantities (normalized by its maximum) for the Three-level amplifier. The value of the fixed parameters are:  $\beta_c = 1$ ,  $\beta_h = 0.1$ ,  $\epsilon_2 = 5$ ,  $\omega_d \in [0.1, 4.9]$ ,  $\gamma_{h/c} \in [10^{-5}, 10^{-2}]$  and  $g \in [10^{-5}, 10^{-3}]$ .

we first define a utility function that depends on the quantities to be optimized (e.g. maximisation of power and minimisation of fluctuations) with the form

$$\Omega := \lambda \langle \dot{W} \rangle - (1 - \lambda) \text{Var}[\dot{W}], \quad (36)$$

where the parameter  $\lambda$  takes values in the range  $[0, 1]$ . The role of the parameter  $\lambda$  is to give weights to the two objectives, thus defining a single optimization problem for the whole function  $\Omega$ . By maximizing  $\Omega$  we obtain solutions that are both optimal in terms of maximizing power and minimizing fluctuations according to a fixed weight  $\lambda$ . For  $\lambda = 0$  we recover the problem of only minimizing fluctuations (whose solution is the zero fluctuations point), while in the case  $\lambda = 1$  we recover the problem of only maximizing power (leading to the maximum power point). Indeed varying  $\lambda$  we obtain a family of standard optimization problems for a single variable,  $\Omega$ . The solution to the multi-objective optimization problem —the so-called Pareto front— is hence constructed by combining the solutions for every single-objective optimization problems, i.e. for all  $\lambda \in [0, 1]$ .

We applied the above optimization technique to the three-level amplifier for numerically obtaining Pareto fronts to three different multi-objective optimization problems, each of which optimizing two of the three performance indicators of the machine, namely average power  $\langle \dot{W} \rangle$ , efficiency  $\eta$  and power fluctuations  $\text{Var}[\dot{W}]$ . In Fig. 6 we can see the shape of the Pareto front (red curves) for the three different optimisation problems with fixed environmental temperatures and varying  $\omega_d$ ,  $\gamma_h$ ,  $\gamma_c$  and  $g$ . There, each circle (independently of its color) is generated from a possible configuration (choice of parameters) of the machine. For the optimization problems involving maximizing power  $\langle \dot{W} \rangle$  and minimizing fluctuations  $\text{Var}[\dot{W}]$  (Fig. 6a) or maximizing power  $\langle \dot{W} \rangle$  and minimizing efficiency  $\eta$  (Fig. 6b), the Pareto fronts include a whole branch of solutions indicating a tradeoff

between the optimization objectives. These go from the zero fluctuations point to the maximum power one in the first case, and from the Carnot point to maximum power point in the second one. On the other hand, for the problem of minimizing fluctuations  $\text{Var}[\dot{W}]$  and maximizing efficiency  $\eta$  (Fig. 6c) the Pareto front collapses to a single point, or optimal solution, achieving zero fluctuations and Carnot efficiency (but at zero output power).

The role of energetic coherence in the performance of the engine can be unveiled by coloring the circles representing each parameter configuration according to their value of the TUR ratio  $Q_{\text{he}}$  (orange for  $Q_{\text{he}} \geq 2$  and blue for TUR violations,  $Q_{\text{he}} < 2$ ). As can be appreciated in Fig. 6, in all cases the configurations that violate the TUR span the domain classically achievable. More importantly, in Figs. 6a and b, we observe TUR violations within the Pareto fronts for large power outputs, and including the maximum power point. This result implies that three level amplifier shows a quantum-thermodynamic advantage (as spotted by the violation of the TUR) in relevant regimes of operation, where the machine performs in an optimal way.

Similarly, we can define and numerically solve the multi-objective optimization problems for the three-qubit refrigerator and NIC machines to obtain their respective Pareto fronts (see Appendix Y). Once all multi-objective optimization problems have been solved for the three quantum thermal machine models, we can compare their optimal solutions with the optimal solutions of their respective classical equivalents. A quantitative comparison of the optimal solutions (Pareto front) in each case, can be performed by computing the difference between the maximum values of their utility functions,  $\Omega - \Omega_{\text{cl}}$ , for a given  $\lambda$ . We focus on the optimisation of  $\langle J_{\text{out}} \rangle$  and  $\text{Var}[J_{\text{out}}]$ , since by construction, the difference between the quantum machine and its classical equivalent lies in the variance of the currents. In Fig. 7 we show

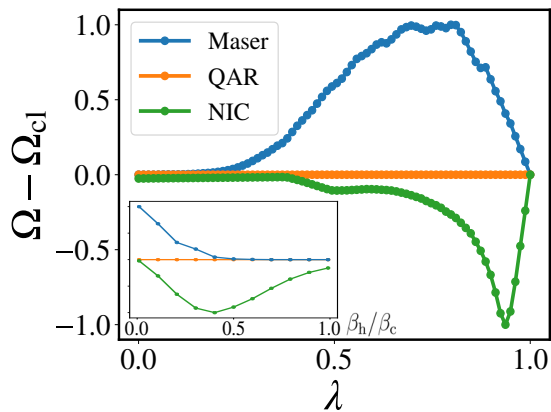


FIG. 7. Difference between the quantum and classical maximums of the utility function  $\Omega$  in the multi-objective optimization of  $\langle \dot{W} \rangle - \text{Var}[\dot{W}]$  as function of  $\lambda$  for fixed environment temperatures (outset plot) and as a function of the environment temperatures for a fixed  $\lambda = 0.8$ . The value of the fixed parameters are:  $\beta_c = 1$ ,  $\epsilon_2 = 5$ ,  $\omega_d \in [0.1, 4.9]$ ,  $\gamma_{h/c} \in [10^{-5}, 10^{-2}]$  and  $g \in [10^{-5}, 10^{-3}]$ .

the behaviour of  $\Omega - \Omega_{cl}$  as a function of  $\lambda$  for the three thermal machine models (and fixed bath temperatures). In all three cases, for small values of  $\lambda$  i.e. close to the zero fluctuations point, we find no difference between the quantum and classical Pareto fronts. However, as soon as  $\lambda$  increases, we find three quite different behaviours: (1) for the three-level amplifier the optimal solution is always better i.e. it reaches greater values of the utility function (that are indeed not achievable in the classical equivalent); (2) for the quantum absorption refrigerator it turns out that there is no difference at all between classical and quantum optimal solutions, hence being these machines exactly equivalent at the level of power, efficiency and stability; (3) the NIC machine is always less optimal than its classical counterpart, specially for high values of  $\lambda$  (high powers) where the NIC machine becomes much noisier than its classical equivalent. In any case, we observe that in the limit  $\lambda = 1$  (maximum power point), for which fluctuations are not taken into account, the optimal solutions of quantum and classical models become equivalent, as expected by construction of the classical equivalent.

Finally, also explore the mismatch in the utility functions,  $\Omega - \Omega_{cl}$ , when varying the temperature bias (see the inset plot in Fig. 7). Fixing the value of  $\lambda$  we observe that the advantages of the three-level amplifier quantum Pareto front are higher for high temperature biases and as we make  $\beta_h/\beta_c$  smaller and smaller they tend to disappear, spotting again a (quantum) non-equilibrium effect. On the other hand, the disadvantages in the NIC machine front do not display a monotonic behavior with the temperature bias and tend to disappear for a high temperature bias, where the quantum and classical models become equally optimal.

## VII. CONCLUSIONS

We have characterized the thermodynamic impact of energetic and degenerate coherence in the performance of quantum thermal machines operating in nonequilibrium steady states. While machines displaying energetic coherence in their steady states can lead to quantum-thermodynamic advantages in terms of their tradeoff between power, efficiency and stability, this is not the case for machines only displaying coherence between degenerate levels, no matter its origin being Hamiltonian or noise-induced. These results, obtained through direct comparison of prototypical quantum thermal machines with axiomatically-constructed classical equivalent models, imply that many previous claims regarding quantum-enhancements in these machines are spurious. Indeed, we showed that even if the dynamics of these machines exhibit purely quantum features (such as e.g. entanglement), a classical Markovian machine using the same set of resources (energy gaps and bath temperatures) can be systematically constructed that performs just as well or better than the original machine. Our results provide, at the same time, an explanation of why violations of the TUR cannot be found in devices showing degenerate coherence.

The classical equivalent model employed here allowed us a comparison of the current fluctuations between a quantum device and a classical (incoherent) counterpart that outputs the same average currents while employing identical thermodynamic resources. This notion of classical equivalent machine constructs on the idea of emulability discussed in Ref. [23], and is accompanied by a general methodology for its derivation in generic cases. The classical equivalent can be constructed for virtually any quantum steady-state machine working in the weak-coupling regime, and under weak-driving conditions, namely, when the driving can be considered a perturbation of the (bare) machine Hamiltonian. Extensions of this method to the case of strong couplings or strong periodic driving (e.g. using Floquet formalism) are an interesting direction for future research which may allow addressing quantum-thermodynamic advantages in a larger class of quantum devices.

Using the three-level amplifier as a main example of a quantum thermal machine displaying energetic coherence, we have shown that it always match or exceeds the performance of its classical equivalent counterpart in all possible configurations, with improvements in the machine stability that become greater for larger temperature bias, i.e. far from equilibrium. The parameter regions where these improvements are maximal coincide indeed with regimes where the thermal machine breaks the TUR bound. Moreover, we also observe wide regions showing (smaller) thermodynamic improvements that are not witnessed by TUR violations. Importantly, our results reveal that in order to observe a truly quantum-thermodynamic advantage in this model, it is necessary (and sufficient) to consider the fluctuations in the cur-

rents (at least at the level of the variance), in contrast to previous assessments based on more limited notions of classical equivalents (leading to a less stringent comparison) [9].

Beyond the direct comparison between quantum machines and their respective equivalents for given parameters, we also provided an all-to-all comparison computing the optimal configurations (Pareto front) of quantum and classical machines maximizing power and efficiency while minimizing fluctuations. Our analysis reveals that quantum-thermodynamic advantages in the three-level amplifier occur indeed within the optimal front, allowing thus for a practical quantum-thermodynamic advantage. Since implementations of this or similar thermal machine models have been proposed in a number of platforms [13, 81], and it has been actually experimentally realized with NV-centers in diamond [12], it would be interesting to test our results for the quantum-thermodynamic advantages reported here in relevant regimes by suitably measuring the variance of the currents [82, 83].

## ACKNOWLEDGMENTS

We thank Roberta Zambrini for comments and interesting discussions. We wish to acknowledge support from the María de Maeztu project CEX2021-001164-M for Units of Excellence and CoQuSy project PID2022-140506NB-C21, funded by MICIU/AEI/10.13039/501100011033/FEDER, UE. GM acknowledges the Ramón y Cajal program RYC2021-031121-I funded by MICIU/AEI/10.13039/501100011033 and European Union NextGenerationEU/PRTR. JAAM acknowledges the Conselleria d'Educació, Universitat i Recerca of the Balearic Islands (Grant FPI FPI.058.2022).

## Appendix A: General expression of current first moments with local dissipation

In this appendix we derive a general expression for the average heat currents including the cases in which coherence may be generated either by Hamiltonian or noise-induced sources. We start by expanding the expression for the standard definition for the heat currents as given in Eq. (13), that is:

$$\begin{aligned} \langle \dot{Q}_r \rangle &= \sum_k \text{Tr}[H_0 \mathcal{D}_k^{(r)}[\pi(t)]] = \sum_k \text{Tr}[\mathcal{D}_k^{\dagger(r)}[H_0]\pi(t)] \\ &= \sum_k \sum_{m,l} \langle m | L_k^{(r)\dagger} H_0 L_k^{(r)} - \frac{1}{2} \{L_k^{(r)\dagger} L_k^{(r)}, H_0\} | l \rangle \pi_{lm} \end{aligned} \quad (\text{A1})$$

where we have applied the cyclic property of the trace to obtain the adjoint dissipator  $\mathcal{D}_k^{\dagger(r)}[\cdot] := L_k^{(r)\dagger} \cdot L_k^{(r)} - \frac{1}{2} \{L_k^{(r)\dagger} L_k^{(r)}, \cdot\}$ . Now, using the explicit form of the Lind-

blad operators in Eq. (4) and the bare Hamiltonian,  $H_0 = \sum_i \epsilon_i |i\rangle \langle i|$ , we can obtain each term in the sum of the last expression:

$$\begin{aligned} L_k^{(r)\dagger} H_0 L_k^{(r)} &= \sum_{i,j,n} \sqrt{\gamma_{ij}\gamma_{nj}} \epsilon_j |i\rangle \langle n| \delta(\Delta\epsilon_{ji} - \Delta\epsilon_k) \delta(\Delta\epsilon_{ni}), \\ L_k^{(r)\dagger} L_k^{(r)} H_0 &= \sum_{i,j,n} \sqrt{\gamma_{ij}\gamma_{nj}} \epsilon_n |i\rangle \langle n| \delta(\Delta\epsilon_{ji} - \Delta\epsilon_k) \delta(\Delta\epsilon_{ni}), \\ H_0 L_k^{(r)\dagger} L_k^{(r)} &= \sum_{i,j,n} \sqrt{\gamma_{ij}\gamma_{nj}} \epsilon_n |n\rangle \langle i| \delta(\Delta\epsilon_{ji} - \Delta\epsilon_k) \delta(\Delta\epsilon_{ni}), \end{aligned} \quad (\text{A2})$$

where the  $\delta$  functions arise from the fact that the Lindblad operators produce jumps only between levels with a fixed energy gap  $\Delta\epsilon_k = \pm\Delta\epsilon_r$ , determined by the reservoirs and we used  $\delta(\Delta\epsilon_{ji} - \Delta\epsilon_k) \delta(\Delta\epsilon_{jn} - \Delta\epsilon_k) = \delta(\Delta\epsilon_{ji} - \Delta\epsilon_k) \delta(\Delta\epsilon_{ji} - \Delta\epsilon_{ij}) = \delta(\Delta\epsilon_{ji} - \Delta\epsilon_k) \delta(\Delta\epsilon_{ni})$ . By introducing the expressions in (A2) into (A1) we arrive at a general expression for the heat currents valid for both degenerate and non-degenerate level structures in the machine:

$$\begin{aligned} \langle \dot{Q}_r \rangle &= \sum_{k,n,i,j} \sqrt{\gamma_{ij}\gamma_{nj}} \delta(\Delta\epsilon_{ji} - \Delta\epsilon_k) \delta(\Delta\epsilon_{ni}) \\ &\quad \times [\epsilon_j \pi_{ni} - \epsilon_n \text{Re}(\pi_{ni})]. \end{aligned} \quad (\text{A3})$$

If we now particularize the above expression for the case where we don't have degenerate energy levels, the term  $\delta(\epsilon_{ni})$  leads to select indices with  $n = i$  and we arrive to:

$$\begin{aligned} \langle \dot{Q}_r \rangle &= \sum_{k,i,j} \delta(\Delta\epsilon_{ji} - \Delta\epsilon_k) (\epsilon_j - \epsilon_i) \gamma_{ij} \pi_{ii} \\ &= \sum_{i < j} (\epsilon_j - \epsilon_i) (\gamma_{ij} \pi_{ii} - \gamma_{ji} \pi_{jj}), \end{aligned} \quad (\text{A4})$$

as given in Eq. (22). On the other hand, for the cases with degenerate energy levels,  $\delta(\epsilon_{ni})$  can be zero even for  $n \neq i$ , and extra terms are obtained. In the case of a single pair of degenerate levels  $|u\rangle$  and  $|v\rangle$  we obtain:

$$\begin{aligned} \langle \dot{Q}_r \rangle &= \sum_{i < j} (\epsilon_j - \epsilon_i) (\gamma_{ij} \pi_{ii} - \gamma_{ji} \pi_{jj}) \\ &\quad + 2 \sum_j (\epsilon_j - \epsilon_v) (\gamma_{uj} + \gamma_{vj}) \text{Re}(\pi_{uv}) \end{aligned} \quad (\text{A5})$$

as we reported in Eq. (27). Notice above that the extra term in the heat current, which is associated to transitions to or from the degenerate levels, is indeed non-zero only in the presence of coherence between the degenerate pair  $\pi_{uv} \neq 0$ . Moreover, the coherence needs to have a real component, as it is the case of the noise-induced coherence machine, c.f. (28). On the other hand, in the case of autonomous refrigerators showing Hamiltonian-induced coherence, the coherence between degenerate levels in the steady state is a pure imaginary number [c.f. Eq. (24)], and the heat current hence reduces to the standard expression for non-degenerate levels, as in Eq. (A4).

## Appendix B: Full Counting Statistics

The Full Counting Statistics (FCS) formalism is used to compute the variances of the different input and output currents of the quantum thermal machines presented and their classical equivalent models. In this formalism a set of counting fields  $\{\chi_r\}$  are introduced that keep track of the exchanges of energy quanta between the machine and the thermal reservoirs  $r$ . These lead to the derivation of a generalized master equation for an extended density operator  $\rho_G(t, \{\chi_r^t\})$  depending on the fields. It reads [78]:

$$\frac{d}{dt}\rho_G(t, \{\chi_r\}) = -i[H(t), \rho_G(t, \{\chi_r\})] + \sum_{r=1}^R \sum_k \bar{\mathcal{D}}_k^{(r)}[\rho_G(t, \{\chi_r\})], \quad (\text{B1})$$

with a new set of dissipators with a modified form:

$$\bar{\mathcal{D}}_k^{(r)}[\rho_G] := \left( e^{-\nu_k^{(r)}\chi_r} L_k^{(r)} \rho_G L_k^{(r)\dagger} - \frac{1}{2} \{L_k^{(r)\dagger} L_k^{(r)}, \rho_G\} \right). \quad (\text{B2})$$

where the numbers  $\nu_k^{(r)}$  are chosen to be 1 for operators  $L_k^{(r)}$  associated with the emission of a quanta into the reservoir  $r$  ( $\Delta\epsilon_k = -\Delta\epsilon_r$ ) and  $-1$  for operators associated with the absorption of a quanta ( $\Delta\epsilon_k = \Delta\epsilon_r$ ). In this way, the counting fields  $\chi_r$  are associated to the net flux of quanta  $\dot{N}_r$  transferred from the reservoir into the machine.

In any case, in the limit  $\{\chi_r\} \rightarrow 0$ , we recover  $\rho_G(t) = \rho(t)$  and (B1) reduces to the standard master equation (2) for the machine evolution. Moreover, as in the case of the original master equation, Eq. (B1) can be linearised and written in the form

$$d\vec{p}_G(t)/dt = W_G(\{\chi_r\})\vec{p}_G(t), \quad (\text{B3})$$

where  $\vec{p}_G(t)$  contains all the density operator elements and  $W_G$  is a matrix capturing the dependence between elements  $\rho_{ij}$  within the set of equations of motion. We are interested in the eigenvalue  $\lambda(\{\chi_r\})$  of the matrix  $W_G$  with the largest real part, which is related to the machine cumulant generating function  $\mathcal{K}(\chi_r, t)$ . Indeed for systems with a single steady state we have that in the long time limit [84]:

$$\mathcal{K}(\{\chi_r\}, t) \rightarrow \lambda(\{\chi_r\})t. \quad (\text{B4})$$

Then the cumulants  $\mathcal{C}_n^{(r)}$  associated to the exchange of quanta with the different reservoirs corresponding to the counting fields  $\chi_r$ , can be obtained as derivatives with respect to that counting fields of this eigenvalue, evaluated for all fields equal to zero:

$$\mathcal{C}_n^{(r)} = (-i\partial_{\chi_r})^n \lambda(\{\chi_l\})|_{\{\chi_l\}=0}, \quad (\text{B5})$$

for  $n = 1, 2, 3, \dots$ . Here the first ( $n = 1$ ) and second ( $n = 2$ ) cumulants correspond, respectively, to the average ( $\mathcal{C}_1^{(r)} = \langle \dot{N}_r \rangle$ ) and variance ( $\mathcal{C}_2^{(r)} = \text{Var}[\dot{N}_r]$ ) of the currents of quanta on that reservoirs. The average and variances of the heat currents in which we are mainly interested in this work are then given by:

$$\langle \dot{Q}_r \rangle = \Delta\epsilon_r \mathcal{C}_1^{(r)}, \quad \text{Var}[\dot{Q}_r] = \Delta\epsilon_r^2 \mathcal{C}_2^{(r)}. \quad (\text{B6})$$

Analogously, the average and variance of the power for the case of the three-level amplifier are given, respectively, by the first law,  $\langle \dot{W} \rangle = \sum_r \langle \dot{Q}_r \rangle$  and in the long-time limit,  $\text{Var}[\dot{W}] = \sum_r \text{Var}[\dot{Q}_r] + 2\text{cov}[\dot{Q}_c \dot{Q}_h] = \omega_d^2 \text{Var}[\dot{N}]$  for  $r = c, h$  where the last equality follows from  $\text{Var}[\dot{Q}_r] = \Delta\epsilon_r^2 \text{Var}[\dot{N}]$  and  $\text{cov}[\dot{Q}_c \dot{Q}_h] = \Delta\epsilon_h \Delta\epsilon_c \text{Var}[\dot{N}]$ .

Unfortunately the size and complexity of the matrix  $W_G$  makes in many cases impossible to obtain analytically the eigenvalue  $\lambda(\{\chi_r\})$  by direct diagonalization of  $W_G$ , and other methods are required. In order to obtain the first and second cumulants analytically, we follow the method known as ‘‘inverse full counting’’ originally introduced in Ref. [79] and used in Refs. [30, 33] for similar purposes. In the following we review this method for the case of a single field  $\chi$ , but the expressions can be naturally extended to multiple fields  $\{\chi_r\}$  as it is our case here (see e.g. appendix C in Ref. [33]).

In this method, the characteristic polynomial of  $W_G$ , namely,  $\text{Pol}(\lambda) := -\det[W_G(\chi) - \lambda\mathbb{1}]$ , is expanded in series in terms of the powers of its eigenvalues:

$$\text{Pol}(\lambda) = \sum_{n=0}^M a_n(\chi) \lambda^n(\chi) = 0, \quad (\text{B7})$$

where  $M$  is the range of the matrix  $W_G$ . Now we define the coefficients:

$$a'_n = i\partial_\chi a_n|_{\chi=0}, \quad (\text{B8})$$

$$a''_n = (i\partial_\chi)^2 a_n|_{\chi=0} = -\partial_\chi^2 a_n|_{\chi=0}, \quad (\text{B9})$$

and similarly denote  $\lambda' = i\partial_\chi \lambda|_{\chi=0}$  and  $\lambda'' = -\partial_\chi^2 \lambda|_{\chi=0}$ . The first derivative of the entire characteristic polynomial is then given by:

$$\left[ i\partial_\chi \sum_n^M a_n \lambda^n \right]_{\chi=0} = \sum_n^M [a'_n + (n+1)a_{n+1}\lambda'] \lambda^n(0), \quad (\text{B10})$$

and the second derivative reads:

$$\begin{aligned} \left[ (-i\partial_\chi)^2 \sum_n^M a_n \lambda^n \right]_{\chi=0} &= \sum_n^M [a''_n + 2(n+1)a'_{n+1}\lambda' \\ &+ (n+1)a_{n+1}\lambda'' + (n+1)(n+2)a_{n+2}\lambda'^2] \lambda^n(0). \end{aligned} \quad (\text{B11})$$

Since  $\text{Pol}(\lambda) = 0$ , both equations above should be equal to zero. Therefore, if the system has a unique steady

state, such that  $\lambda(0) = 0$ , as it is our case, then the zero order term in  $\lambda$  vanish, and we obtain from (B10):

$$a'_0 + a_1 \lambda' = 0, \quad (\text{B12})$$

so that the first cumulant (average current) is given by:

$$C_1 = \lambda' = -\frac{a'_0}{a_1}, \quad (\text{B13})$$

and in the same way from (B11) we obtain the second cumulant (variance):

$$C_2 = \frac{2(a'_0 a_1 a'_1 - a_0'^2 a_1') - a_0'' a_1^2}{a_1^3}. \quad (\text{B14})$$

In the following we provide the form of the matrix  $W_G$  for the three quantum thermal machines used as main illustrative examples in this paper and their corresponding classical equivalents. The corresponding expressions for the cumulants are, however, not included here for size reasons.

### 1. Three-level coherent amplifier

To obtain the form of  $W_G$  for this case, we write the system of equations for all elements of  $\rho_G$  given by (B1), using the Hamiltonian and Lindblad operators given in

Sec. II A. We consider only the relevant elements of the matrix leading to non-zero values of the density operator  $\pi$  in the steady state. That is, we include terms connecting the level populations and the imaginary part of the coherence between states  $|0\rangle$  and  $|1\rangle$  (see Appendix C). On the other hand, both the real part of  $\pi_{12}$  and the real and imaginary part of the other coherences  $\pi_{13}$  and  $\pi_{23}$  become zero at the steady state and we don't need to describe their evolution. The matrix reads:

$$W_G = \begin{pmatrix} -\gamma_{02} & 0 & \gamma_{20} e^{-i\chi_h} & 2g \\ 0 & -\gamma_{12} & \gamma_{21} e^{-i\chi_c} & -2g \\ \gamma_{02} e^{i\chi_h} & \gamma_{12} e^{i\chi_c} & -(\gamma_{20} + \gamma_{21}) & 0 \\ g & -g & 0 & -\frac{1}{2}(\gamma_{02} + \gamma_{01}) \end{pmatrix},$$

associated to vector  $\vec{p}_G(t) = (\rho_{00}, \rho_{11}, \rho_{22}, \text{Im}[\rho_{01}])$ . In the case of the classical equivalent, we no longer consider the contribution of coherence to the dynamics, but introduce the classical stochastic transition rate between the interacting levels, leading to a matrix  $W_G^{\text{cl}}$  that reads:

$$W_G^{\text{cl}} = \begin{pmatrix} -(\gamma_{02} - \gamma_{10}^{\text{cl}}) & \gamma_{10}^{\text{cl}} & \gamma_{20} e^{-i\chi_h} \\ \gamma_{10}^{\text{cl}} & -(\gamma_{12} + \gamma_{10}^{\text{cl}}) & \gamma_{21} e^{-i\chi_c} \\ \gamma_{02} e^{i\chi_h} & \gamma_{12} e^{i\chi_c} & -(\gamma_{20} + \gamma_{21}) \end{pmatrix},$$

with the corresponding associated vector  $\vec{p}_G^{\text{cl}}(t) = (\rho_{00}, \rho_{11}, \rho_{22})$ .

### 2. Three-qubit autonomous refrigerator

Using the Hamiltonian and the Lindblad operators given in Sec. II B, we can derive in an analogous way the  $W_G$  matrices for the autonomous absorption refrigerator and its classical equivalent. Here again, we consider only relevant elements of the density matrix, which now consist of the populations of the 8 energy levels (in the three-qubit composed ladder) and a pure imaginary coherence between the states  $|101\rangle$  and  $|010\rangle$ . The  $W_G$  matrix now have the form:

$$W_G = \begin{pmatrix} \Gamma_1 & \gamma_{10}^h e^{-i\chi_h} & \gamma_{10}^c e^{-i\chi_c} & 0 & 0 & 0 & 0 & \gamma_{10}^m e^{-i\chi_m} & 0 \\ \gamma_{01}^h e^{i\chi_h} & \Gamma_2 & 0 & \gamma_{10}^m e^{-i\chi_m} & 0 & 0 & \gamma_{10}^c e^{-i\chi_c} & 0 & 0 \\ \gamma_{01}^c e^{i\chi_c} & 0 & \Gamma_3 & 0 & \gamma_{10}^m e^{-i\chi_m} & 0 & \gamma_{10}^h e^{-i\chi_h} & 0 & 0 \\ 0 & \gamma_{01}^m e^{i\chi_m} & 0 & \Gamma_4 & 0 & \gamma_{10}^c e^{-i\chi_c} & 0 & \gamma_{01}^h e^{i\chi_h} & 0 \\ 0 & 0 & \gamma_{01}^m e^{i\chi_m} & 0 & \Gamma_5 & \gamma_{10}^h e^{-i\chi_h} & 0 & \gamma_{01}^c e^{i\chi_c} & 0 \\ 0 & 0 & 0 & \gamma_{01}^c e^{i\chi_c} & \gamma_{01}^h e^{i\chi_h} & \Gamma_6 & \gamma_{01}^m e^{i\chi_m} & 0 & 0 \\ 0 & \gamma_{01}^c e^{i\chi_c} & \gamma_{01}^h e^{i\chi_h} & 0 & 0 & \gamma_{10}^m e^{-i\chi_m} & \Gamma_7 & 0 & g \\ \gamma_{01}^m e^{i\chi_m} & 0 & 0 & \gamma_{10}^h e^{-i\chi_h} & \gamma_{10}^c e^{-i\chi_c} & 0 & 0 & \Gamma_8 & -g \\ 0 & 0 & 0 & 0 & 0 & 0 & -g & g & \Gamma_9 \end{pmatrix}$$



associated to vector  $\vec{p}_G(t) = (\rho_{000}, \rho_{001}, \rho_{100}, \rho_{011}, \rho_{111}, \rho_{101}, \rho_{010}, \text{Im}[\rho_{010-101}])$ . For the classical equivalent we instead loose the coherence contribution, while adding the extra rate  $\gamma^{\text{cl}}$  between degenerated levels:

$$W_G^{\text{cl}} = \begin{pmatrix} \Gamma_1 & \gamma_{10}^{\text{h}} e^{-i\chi_{\text{h}}} & \gamma_{10}^{\text{c}} e^{-i\chi_{\text{c}}} & 0 & 0 & 0 & 0 & \gamma_{10}^{\text{m}} e^{-i\chi_{\text{m}}} \\ \gamma_{01}^{\text{h}} e^{i\chi_{\text{h}}} & \Gamma_2 & 0 & \gamma_{10}^{\text{m}} e^{-i\chi_{\text{m}}} & 0 & 0 & \gamma_{10}^{\text{c}} e^{-i\chi_{\text{c}}} & 0 \\ \gamma_{01}^{\text{c}} e^{i\chi_{\text{c}}} & 0 & \Gamma_3 & 0 & \gamma_{10}^{\text{m}} e^{-i\chi_{\text{m}}} & 0 & \gamma_{10}^{\text{h}} e^{-i\chi_{\text{h}}} & 0 \\ 0 & \gamma_{01}^{\text{m}} e^{i\chi_{\text{m}}} & 0 & \Gamma_4 & 0 & \gamma_{10}^{\text{c}} e^{-i\chi_{\text{c}}} & 0 & \gamma_{01}^{\text{h}} e^{i\chi_{\text{h}}} \\ 0 & 0 & \gamma_{01}^{\text{m}} e^{i\chi_{\text{m}}} & 0 & \Gamma_5 & \gamma_{10}^{\text{h}} e^{-i\chi_{\text{h}}} & 0 & \gamma_{01}^{\text{c}} e^{i\chi_{\text{c}}} \\ 0 & 0 & 0 & \gamma_{01}^{\text{c}} e^{i\chi_{\text{c}}} & \gamma_{01}^{\text{h}} e^{i\chi_{\text{h}}} & \Gamma_6 & \gamma_{01}^{\text{m}} e^{i\chi_{\text{m}}} & 0 \\ 0 & \gamma_{01}^{\text{c}} e^{i\chi_{\text{c}}} & \gamma_{01}^{\text{h}} e^{i\chi_{\text{h}}} & 0 & 0 & \gamma_{10}^{\text{m}} e^{-i\chi_{\text{m}}} & \Gamma_7 - \gamma^{\text{cl}} & \gamma^{\text{cl}} \\ \gamma_{01}^{\text{m}} e^{i\chi_{\text{m}}} & 0 & 0 & \gamma_{10}^{\text{h}} e^{-i\chi_{\text{h}}} & \gamma_{10}^{\text{c}} e^{-i\chi_{\text{c}}} & 0 & \gamma^{\text{cl}} & \Gamma_8 - \gamma^{\text{cl}} \end{pmatrix}$$

for vector  $\vec{p}_G^{\text{cl}}(t) = (\rho_{000}, \rho_{001}, \rho_{100}, \rho_{011}, \rho_{111}, \rho_{101}, \rho_{010})$ . In the above equations, we defined  $\Gamma_1 = -(\gamma_{01}^{\text{c}} + \gamma_{01}^{\text{m}} + \gamma_{01}^{\text{h}})$ ,  $\Gamma_2 = -(\gamma_{01}^{\text{c}} + \gamma_{01}^{\text{m}} + \gamma_{10}^{\text{h}})$ ,  $\Gamma_3 = -(\gamma_{10}^{\text{c}} + \gamma_{01}^{\text{m}} + \gamma_{01}^{\text{h}})$ ,  $\Gamma_4 = -(\gamma_{01}^{\text{c}} + \gamma_{10}^{\text{m}} + \gamma_{10}^{\text{h}})$ ,  $\Gamma_5 = -(\gamma_{10}^{\text{c}} + \gamma_{10}^{\text{m}} + \gamma_{01}^{\text{h}})$ ,  $\Gamma_6 = -(\gamma_{10}^{\text{c}} + \gamma_{10}^{\text{m}} + \gamma_{10}^{\text{h}})$ ,  $\Gamma_7 = -(\gamma_{10}^{\text{c}} + \gamma_{01}^{\text{m}} + \gamma_{10}^{\text{h}})$ ,  $\Gamma_8 = -(\gamma_{01}^{\text{c}} + \gamma_{10}^{\text{m}} + \gamma_{01}^{\text{h}})$  and  $\Gamma_9 = -\frac{1}{2}(\gamma_{\text{d}} + \gamma_{2\text{d}} + \gamma_{3\text{d}} + \gamma_{\text{u}} + \gamma_{2\text{u}} + \gamma_{3\text{u}})$ .

### 3. Noise-induced-coherent machine

Finally, using the Hamiltonian and Lindblad operators from Sec. II C, we obtain the generic form of  $W_G$  for the noise-induced-coherence machine. In contrast with the previous cases, now we obtain non-zero real coherence in the steady state between states  $|\alpha\rangle$  and  $|\beta\rangle$  (see Appendix C). The relevant elements of the  $W_G$  matrix then connect the populations of the four levels and the real part of the coherence between states  $|\alpha\rangle$  and  $|\beta\rangle$ :

$$W_G = \begin{pmatrix} -(\gamma_{0\alpha} + \gamma_{01}) & \gamma_{10} e^{-i\chi_{\text{w}}} & \gamma_{\alpha 0} e^{-i\chi_{\text{c}}} & 0 & 0 \\ \gamma_{01} e^{i\chi_{\text{w}}} & -(\gamma_{1\alpha} + \gamma_{1\beta} + \gamma_{10}) & \gamma_{\alpha 1} e^{-i\chi_{\text{h}}} & \gamma_{\beta 1} e^{-i\chi_{\text{h}}} & 2\sqrt{\gamma_{\alpha 1}\gamma_{\beta 1}} \\ \gamma_{0\alpha} e^{i\chi_{\text{c}}} & \gamma_{1\alpha} e^{i\chi_{\text{h}}} & -(\gamma_{\alpha 1} + \gamma_{\alpha 0}) & 0 & -\sqrt{\gamma_{\alpha 1}\gamma_{\beta 1}} \\ 0 & \gamma_{1\beta} e^{i\chi_{\text{h}}} & 0 & -\gamma_{\beta 1} & -\sqrt{\gamma_{\alpha 1}\gamma_{\beta 1}} \\ 0 & 2\sqrt{\gamma_{1\alpha}\gamma_{1\beta}} & -\sqrt{\gamma_{\alpha 1}\gamma_{\beta 1}} & -\sqrt{\gamma_{\alpha 1}\gamma_{\beta 1}} & \gamma_{\alpha 0} + \gamma_{\alpha 1} + \gamma_{\beta 1} \end{pmatrix},$$

with  $\vec{p}_G(t) = (\rho_{00}, \rho_{11}, \rho_{\alpha\alpha}, \rho_{\beta\beta}, \text{Re}[\rho_{\alpha\beta}])$ . The matrix for the classical equivalent of the NIC machine does not contain the coherence anymore, but the modified rates  $\{\gamma_{1\alpha}^{\text{cl}}, \gamma_{\alpha 1}^{\text{cl}}, \gamma_{1\beta}^{\text{cl}}, \gamma_{\beta 1}^{\text{cl}}, \gamma_{\alpha\beta}^{\text{cl}}\}$ . It reads:

$$W_G^{\text{cl}} = \begin{pmatrix} -(\gamma_{0\alpha} + \gamma_{01}) & \gamma_{10} e^{-i\chi_{\text{w}}} & \gamma_{\alpha 0} e^{-i\chi_{\text{c}}} & 0 \\ \gamma_{01} e^{i\chi_{\text{w}}} & -(\gamma_{1\alpha}^{\text{cl}} + \gamma_{1\beta}^{\text{cl}} + \gamma_{10}) & \gamma_{\alpha 1}^{\text{cl}} e^{-i\chi_{\text{h}}} & \gamma_{\beta 1}^{\text{cl}} e^{-i\chi_{\text{h}}} \\ \gamma_{0\alpha} e^{i\chi_{\text{c}}} & \gamma_{1\alpha}^{\text{cl}} e^{i\chi_{\text{h}}} & -(\gamma_{\alpha 1}^{\text{cl}} + \gamma_{\alpha 0} + \gamma_{\alpha\beta}^{\text{cl}}) & \gamma_{\alpha\beta}^{\text{cl}} \\ 0 & \gamma_{1\beta}^{\text{cl}} e^{i\chi_{\text{h}}} & \gamma_{\alpha\beta}^{\text{cl}} & -(\gamma_{\beta 1}^{\text{cl}} + \gamma_{\alpha\beta}^{\text{cl}}) \end{pmatrix},$$

with associated vector  $\vec{p}_G^{\text{cl}}(t) = (\rho_{00}, \rho_{11}, \rho_{\alpha\alpha}, \rho_{\beta\beta})$ .

#### Appendix C: Classical thermodynamic-equivalent models details

In this appendix we provide details on the procedure followed to obtain a classical thermodynamically equivalent model, in both cases of Hamiltonian-induced and noise-induced coherences. Moreover, we show that, even in the case of noise-induced coherence, it is sufficient that the classical analogue reproduces the steady-state populations in order to produce exactly the same steady state average currents.

We start by obtaining the equations of motion for the density operator elements from the master equation in Lindblad form (2), from which we can obtain the expres-

sion for a generic element of the density operator:

$$\dot{\rho}_{ij} = -i \langle i | [H(t), \rho] | j \rangle + \sum_r \sum_k \langle i | \mathcal{D}_k^{(r)}[\rho] | j \rangle. \quad (\text{C1})$$

After expanding the form of the dissipators  $\mathcal{D}_k^{(r)}[\rho] = L_k^{(r)} \rho L_k^{(r)\dagger} - \frac{1}{2} \{L_k^{(r)\dagger} L_k^{(r)}, \rho\}$ , we obtain the following

terms contributing to the above expression:

$$\begin{aligned}
\langle i | [H(t), \rho] | j \rangle &= (\epsilon_j - \epsilon_i) \rho_{ij} + g(\delta_{iu} \rho_{vj} + \delta_{iv} \rho_{uj} \\
&\quad - \delta_{vj} \rho_{iu} - \delta_{uj} \rho_{iv}), \\
\langle i | L_k^{(r)} \rho L_k^{(r)\dagger} | j \rangle &= \sum_{n,m} \alpha_{ni}^k \alpha_{mj}^k \sqrt{\gamma_{ni} \gamma_{mj}} \rho_{nm}, \\
\langle i | L_k^{(r)\dagger} L_k^{(r)} \rho | j \rangle &= \sum_{n,m} \alpha_{im}^k \alpha_{nm}^k \sqrt{\gamma_{im} \gamma_{nm}} \rho_{nj}, \\
\langle i | \rho L_k^{(r)\dagger} L_k^{(r)} | j \rangle &= \sum_{n,m} \alpha_{nm}^k \alpha_{jm}^k \sqrt{\gamma_{nm} \gamma_{jm}} \rho_{in},
\end{aligned} \tag{C2}$$

where we can again use the fact that the Lindblad operators produce jumps only between levels with a fixed energy gap  $\Delta\epsilon_k = \pm\Delta\epsilon_r$ , determined by the reservoirs and rewrite the  $\alpha$ -terms as delta functions:

$$\begin{aligned}
\alpha_{ni}^k \alpha_{mj}^k &= \delta(\Delta\epsilon_{in} - \Delta\epsilon_k) \delta(\Delta\epsilon_{jm} - \Delta\epsilon_k), \\
\alpha_{im}^k \alpha_{nm}^k &= \delta(\Delta\epsilon_{mi} - \Delta\epsilon_k) \delta(\Delta\epsilon_{ni}), \\
\alpha_{nm}^k \alpha_{jm}^k &= \delta(\Delta\epsilon_{mn} - \Delta\epsilon_k) \delta(\Delta\epsilon_{nj}).
\end{aligned} \tag{C3}$$

To specialize this result for the case of Hamiltonian-induced coherence we can use the fact that in (C2) first expression the only non-zero part is the second term, since the first will vanish, because we can always go to the interaction picture and consider only the interaction term of the total Hamiltonian (or in the non-energetic case both interacting levels have the same energy). On the other hand, the  $\delta$  functions in (C3) can be simplified by taking into account the fact that in this case different transitions cannot have the same  $\Delta\epsilon_k$  associated with them. Then (C3) becomes:

$$\begin{aligned}
\alpha_{ni}^k \alpha_{mj}^k &= \delta(\Delta\epsilon_{in} - \Delta\epsilon_k) \delta_{ij} \delta_{nm}, \\
\alpha_{im}^k \alpha_{nm}^k &= \delta(\Delta\epsilon_{mi} - \Delta\epsilon_k) \delta_{ni}, \\
\alpha_{nm}^k \alpha_{jm}^k &= \delta(\Delta\epsilon_{mn} - \Delta\epsilon_k) \delta_{nj}.
\end{aligned} \tag{C4}$$

which results in the set of equations (23).

In the case of noise-induced coherence, we don't have an interaction Hamiltonian, so the first expression on (C2) doesn't need to be considered. The  $\delta$  functions in (C3), on the other hand, have more terms, since there are now different transitions associated with the same  $\Delta\epsilon_k$ .

Now (C3) reads:

$$\begin{aligned}
\alpha_{ni}^k \alpha_{mj}^k &= \delta(\Delta\epsilon_{in} - \Delta\epsilon_k) (\delta_{ij} \delta_{nm} + \delta_{iu} \delta_{jv} \delta_{nm} + \delta_{iv} \delta_{ju} \delta_{nm} \\
&\quad + \delta_{nu} \delta_{mv} \delta_{ij} + \delta_{nv} \delta_{mu} \delta_{ij}), \\
\alpha_{im}^k \alpha_{nm}^k &= \delta(\Delta\epsilon_{mi} - \Delta\epsilon_k) (\delta_{ni} + \delta_{iv} \delta_{nu} + \delta_{iu} \delta_{nv}), \\
\alpha_{nm}^k \alpha_{jm}^k &= \delta(\Delta\epsilon_{mn} - \Delta\epsilon_k) (\delta_{nj} + \delta_{jv} \delta_{nu} + \delta_{ju} \delta_{nv}).
\end{aligned} \tag{C5}$$

In view of (C5) the equations of motion are:

$$\dot{\rho}_{nn} = \sum_i (\gamma_{in} \rho_{ii} - \gamma_{ni} \rho_{nn}) + 2\sqrt{\gamma_{un} \gamma_{vn}} \text{Re}(\rho_{uv}), \tag{C6}$$

for the levels  $n \neq \{u, v\}$ , and:

$$\begin{aligned}
\dot{\rho}_{nn} &= \sum_i [\gamma_{in} \rho_{ii} - (\gamma_{ni} \rho_{nn} + \sqrt{\gamma_{ui} \gamma_{vi}} \text{Re}(\rho_{uv}))], \\
\dot{\rho}_{uv} &= \sum_i [2\sqrt{\gamma_{iu} \gamma_{iv}} \rho_{ii} - \sqrt{\gamma_{ui} \gamma_{vi}} (\rho_{uu} + \rho_{vv}) \\
&\quad - (\gamma_{ui} + \gamma_{vi}) \rho_{uv}].
\end{aligned} \tag{C7}$$

for  $n = \{u, v\}$ . They result in a steady-state coherence term given by (28) where the introduction of (28) into (C7) leads to corrections for rates and a new transition between levels  $u$  and  $v$  as shown in (29).

Finally, we show that all energy currents in the quantum machine and the classical equivalent are equal, also in the case of noise-induced coherence. Taking into account the fact that the transition in contact with the "work" reservoir is not involved in the noise inducing mechanism (involving only transitions from or to the degenerate levels), we observe that the classical equivalent can mimic the current  $\langle \dot{Q}_w \rangle$  in the original machine if it has the same populations in the steady state (since Eq. (22) depends only on the populations of the density matrix). Then, using Eq. (16), we also have that

$$\langle \dot{Q}_w \rangle = \langle \dot{Q}_w^{\text{cl}} \rangle \implies \langle \dot{N} \rangle = \langle \dot{N}^{\text{cl}} \rangle, \tag{C8}$$

$\langle \dot{N}^{\text{cl}} \rangle$  being the corresponding probability current in the classical equivalent machine. The above relation stating the equivalence of the steady-state probability currents in quantum and classical engines implies, at the same time, that all the other energy currents in the original and classical equivalent machines are equal to their classical counterparts.

- 
- [1] F. Binder, L. A. Correa, C. Gogolin, J. Anders, and G. Adesso, eds., *Thermodynamics in the Quantum Regime* (Springer, Cham, 2018).  
[2] G. T. Landi and M. Paternostro, Irreversible entropy production: From classical to quantum, *Rev. Mod. Phys.* **93**, 035008 (2021).  
[3] H. E. D. Scovil and E. O. Schulz-DuBois, Three-level

- masers as heat engines, *Phys. Rev. Lett.* **2**, 262 (1959).  
[4] E. Geva and R. Kosloff, Three-level quantum amplifier as a heat engine: A study in finite-time thermodynamics, *Phys. Rev. E* **49**, 3903 (1994).  
[5] E. Boukobza and D. J. Tannor, Three-level systems as amplifiers and attenuators: A thermodynamic analysis, *Phys. Rev. Lett.* **98**, 240601 (2007).

- [6] N. Linden, S. Popescu, and P. Skrzypczyk, How small can thermal machines be? the smallest possible refrigerator, *Phys. Rev. Lett.* **105**, 130401 (2010).
- [7] A. Levy and R. Kosloff, Quantum absorption refrigerator, *Phys. Rev. Lett.* **108**, 070604 (2012).
- [8] N. Brunner, N. Linden, S. Popescu, and P. Skrzypczyk, Virtual qubits, virtual temperatures, and the foundations of thermodynamics, *Phys. Rev. E* **85**, 051117 (2012).
- [9] R. Uzdin, A. Levy, and R. Kosloff, Equivalence of quantum heat machines, and quantum-thermodynamic signatures, *Phys. Rev. X* **5**, 031044 (2015).
- [10] J. Roßnagel, S. T. Dawkins, K. N. Tolazzi, O. Abah, E. Lutz, F. Schmidt-Kaler, and K. Singer, A single-atom heat engine, *Science* **352**, 325 (2016).
- [11] G. Maslennikov, S. Ding, R. Hablutzel, J. Gan, A. Roulet, S. Nimmrichter, J. Dai, V. Scarani, and D. Matsukevich, Quantum absorption refrigerator with trapped ions, *Nat. Commun.* **10**, 202 (2019).
- [12] J. Klatzow, J. N. Becker, P. M. Ledingham, C. Weinzetl, K. T. Kaczmarek, D. J. Saunders, J. Nunn, I. A. Walmsley, R. Uzdin, and E. Poem, Experimental demonstration of quantum effects in the operation of microscopic heat engines, *Phys. Rev. Lett.* **122**, 110601 (2019).
- [13] N. M. Myers, O. Abah, and S. Deffner, Quantum thermodynamic devices: From theoretical proposals to experimental reality, *AVS Quantum Science* **4**, 027101 (2022), [https://pubs.aip.org/avs/aqs/article-pdf/doi/10.1116/5.0083192/16494008/027101\\_1.online.pdf](https://pubs.aip.org/avs/aqs/article-pdf/doi/10.1116/5.0083192/16494008/027101_1.online.pdf).
- [14] M. O. Scully, M. S. Zubairy, G. S. Agarwal, and H. Walther, Extracting work from a single heat bath via vanishing quantum coherence, *Science* **299**, 862 (2003), <https://www.science.org/doi/pdf/10.1126/science.1078955>.
- [15] R. Kosloff and A. Levy, Quantum heat engines and refrigerators: Continuous devices, *Annu. Rev. Phys. Chem.* **65**, 365 (2014).
- [16] M. O. Scully, K. R. Chapin, K. E. Dorfman, M. B. Kim, and A. Svidzinsky, Quantum heat engine power can be increased by noise-induced coherence, *Proceedings of the National Academy of Sciences* **108**, 15097 (2011), <https://www.pnas.org/doi/pdf/10.1073/pnas.1110234108>.
- [17] D. Gelbwaser-Klimovsky, W. Niedenzu, P. Brumer, and G. Kurizki, Power enhancement of heat engines via correlated thermalization in a three-level working fluid, *Sci. Rep.* **5**, 14413 (2015).
- [18] J. Um, K. E. Dorfman, and H. Park, Coherence-enhanced quantum-dot heat engine, *Phys. Rev. Res.* **4**, L032034 (2022).
- [19] K. E. Dorfman, D. V. Voronine, S. Mukamel, and M. O. Scully, Photosynthetic reaction center as a quantum heat engine, *Proceedings of the National Academy of Sciences* **110**, 2746 (2013), <https://www.pnas.org/doi/pdf/10.1073/pnas.1212666110>.
- [20] N. Brunner, M. Huber, N. Linden, S. Popescu, R. Silva, and P. Skrzypczyk, Entanglement enhances cooling in microscopic quantum refrigerators, *Phys. Rev. E* **89**, 032115 (2014).
- [21] M. T. Mitchison, M. P. Woods, J. Prior, and M. Huber, Coherence-assisted single-shot cooling by quantum absorption refrigerators, *New Journal of Physics* **17**, 115013 (2015).
- [22] G. Manzano, G.-L. Giorgi, R. Fazio, and R. Zambrini, Boosting the performance of small autonomous refrigerators via common environmental effects, *New Journal of Physics* **21**, 123026 (2019).
- [23] J. O. González, J. P. Palao, D. Alonso, and L. A. Correa, Classical emulation of quantum-coherent thermal machines, *Phys. Rev. E* **99**, 062102 (2019).
- [24] A. C. Barato and U. Seifert, Thermodynamic uncertainty relation for biomolecular processes, *Phys. Rev. Lett.* **114**, 158101 (2015).
- [25] T. R. Gingrich, J. M. Horowitz, N. Perunov, and J. L. England, Dissipation bounds all steady-state fluctuations, *Phys. Rev. Lett.* **116**, 120601 (2016).
- [26] J. M. Horowitz and T. R. Gingrich, Thermodynamic uncertainty relations constrain non-equilibrium fluctuations, *Nat. Phys.* **16**, 15 (2020).
- [27] P. Pietzonka and U. Seifert, Universal trade-off between power, efficiency, and constancy in steady-state heat engines, *Phys. Rev. Lett.* **120**, 190602 (2018).
- [28] K. Ptaszyński, Coherence-enhanced constancy of a quantum thermoelectric generator, *Phys. Rev. B* **98**, 085425 (2018).
- [29] J. Liu and D. Segal, Thermodynamic uncertainty relation in quantum thermoelectric junctions, *Phys. Rev. E* **99**, 062141 (2019).
- [30] A. A. S. Kalae, A. Wacker, and P. P. Potts, Violating the thermodynamic uncertainty relation in the three-level maser, *Phys. Rev. E* **104**, L012103 (2021).
- [31] A. Rignon-Bret, G. Guarnieri, J. Gould, and M. T. Mitchison, Thermodynamics of precision in quantum nanomachines, *Phys. Rev. E* **103**, 012133 (2021).
- [32] L. d. S. Souza, G. Manzano, R. Fazio, and F. Iemini, Collective effects on the performance and stability of quantum heat engines, *Phys. Rev. E* **106**, 014143 (2022).
- [33] G. Manzano and R. López, Quantum-enhanced performance in superconducting andreev reflection engines, *Phys. Rev. Res.* **5**, 043041 (2023).
- [34] L. F. Seoane and R. V. Solé, A multiobjective optimization approach to statistical mechanics, *arXiv: Statistical Mechanics* (2013).
- [35] L. Dinis, J. Unterberger, and D. Lacoste, Phase transitions in optimal betting strategies, *Europhysics Letters* **131**, 60005 (2020).
- [36] L. Dinis, J. Unterberger, and D. Lacoste, Pareto-optimal trade-off for phenotypic switching of populations in a stochastic environment, *Journal of Statistical Mechanics: Theory and Experiment* **2022**, 053503 (2022).
- [37] A. P. Solon and J. M. Horowitz, Phase transition in protocols minimizing work fluctuations, *Phys. Rev. Lett.* **120**, 180605 (2018).
- [38] P. A. Erdman, A. Rolandi, P. Abiuso, M. Perarnau-Llobet, and F. Noé, Pareto-optimal cycles for power, efficiency and fluctuations of quantum heat engines using reinforcement learning, *Phys. Rev. Res.* **5**, L022017 (2023).
- [39] H. J. D. Miller and M. Mehboudi, Geometry of work fluctuations versus efficiency in microscopic thermal machines, *Phys. Rev. Lett.* **125**, 260602 (2020).
- [40] H.-P. Breuer and F. Petruccione, *The Theory of Open Quantum Systems* (OXFORD University Press, 2002).
- [41] Ángel Rivas and S. F. Huelga, *Open Quantum Systems. An introduction* (Springer, 2012).
- [42] G. D. Chiara, G. Landi, A. Hewgill, B. Reid, A. Ferraro, A. J. Roncaglia, and M. Antezza, Reconciliation of quantum local master equations with thermodynamics, *New Journal of Physics* **20**, 113024 (2018).
- [43] P. P. Hofer, M. Perarnau-Llobet, L. D. M. Miranda, G. Haack, R. Silva, J. B. Brask, and N. Brunner, Marko-

- vian master equations for quantum thermal machines: local versus global approach, *New Journal of Physics* **19**, 123037 (2017).
- [44] A. S. Trushechkin and I. V. Volovich, Perturbative treatment of inter-site couplings in the local description of open quantum networks, *Europhysics Letters* **113**, 30005 (2016).
- [45] J. E. Geusic, E. O. Schulz-DuBios, and H. E. D. Scovil, Quantum equivalent of the carnot cycle, *Phys. Rev.* **156**, 343 (1967).
- [46] J. P. Palao, R. Kosloff, and J. M. Gordon, Quantum thermodynamic cooling cycle, *Phys. Rev. E* **64**, 056130 (2001).
- [47] S.-W. Li, M. B. Kim, G. S. Agarwal, and M. O. Scully, Quantum statistics of a single-atom scovil–schulz-dubois heat engine, *Phys. Rev. A* **96**, 063806 (2017).
- [48] E. D. Konstantin, X. Dazhi, and C. Jianshu, Efficiency at maximum power of a laser quantum heat engine enhanced by noise-induced coherence., *Phys. Rev. E* **97** (2018).
- [49] S. Varinder, Optimal operation of a three-level quantum heat engine and universal nature of efficiency., *Phys. Rev. Research* **2** (2020).
- [50] P. Skrzypczyk, N. Brunner, N. Linden, and S. Popescu, The smallest refrigerators can reach maximal efficiency, *Journal of Physics A: Mathematical and Theoretical* **44**, 492002 (2011).
- [51] R. Silva, G. Manzano, P. Skrzypczyk, and N. Brunner, Performance of autonomous quantum thermal machines: Hilbert space dimension as a thermodynamical resource, *Phys. Rev. E* **94**, 032120 (2016).
- [52] L. A. Correa, J. P. Palao, G. Adesso, and D. Alonso, Performance bound for quantum absorption refrigerators, *Phys. Rev. E* **87**, 042131 (2013).
- [53] C. L. A., P. J. P., A. Gerardo, and A. Daniel, Optimal performance of endoreversible quantum refrigerators., *Phys. Rev. E* **90** (2014).
- [54] L. A. Correa, J. P. Palao, D. Alonso, and G. Adesso, Quantum-enhanced absorption refrigerators, *Scientific Reports* **21** (2014).
- [55] S. Seah, S. Nimmrichter, and V. Scarani, Refrigeration beyond weak internal coupling, *Phys. Rev. E* **98**, 012131 (2018).
- [56] D. Venturelli, R. Fazio, and V. Giovannetti, Minimal self-contained quantum refrigeration machine based on four quantum dots, *Phys. Rev. Lett.* **110**, 256801 (2013).
- [57] M. T. Mitchison, M. Huber, J. Prior, M. P. Woods, and M. B. Plenio, Realising a quantum absorption refrigerator with an atom-cavity system, *Quantum Science and Technology* **1**, 015001 (2016).
- [58] P. P. Hofer, M. Perarnau-Llobet, J. B. Brask, R. Silva, M. Huber, and N. Brunner, Autonomous quantum refrigerator in a circuit qed architecture based on a josephson junction, *Phys. Rev. B* **94**, 235420 (2016).
- [59] M. O. Scully, Quantum photocell: Using quantum coherence to reduce radiative recombination and increase efficiency, *Phys. Rev. Lett.* **104**, 207701 (2010).
- [60] V. V. Kozlov, Y. Rostovtsev, and M. O. Scully, Inducing quantum coherence via decays and incoherent pumping with application to population trapping, lasing without inversion, and quenching of spontaneous emission, *Phys. Rev. A* **74**, 063829 (2006).
- [61] T. V. Tscherbul and P. Brumer, Long-lived quasistationary coherences in a v-type system driven by incoherent light., *Phys. Rev. Lett.* **113** (2014).
- [62] U. Harbola, S. Rahav, and S. Mukamel, Quantum heat engines: A thermodynamic analysis of power and efficiency, *Europhysics Letters* **99**, 50005 (2012).
- [63] H. P. Goswami and U. Harbola, Thermodynamics of quantum heat engines, *Phys. Rev. A* **88**, 013842 (2013).
- [64] N. Killoran, S. F. Huelga, and M. B. Plenio, Enhancing light-harvesting power with coherent vibrational interactions: A quantum heat engine picture., *J. Chem. Phys.* **143** (2015).
- [65] C.-P. S. Shan-He Su, S.-W. Li, and J.-C. Chen, Photoelectric converters with quantum coherence., *Phys. Rev. E* **93** (2016).
- [66] V. Holubec and T. Novotný, Effects of noise-induced coherence on the performance of quantum absorption refrigerators., *J. Low Temp. Phys.* **192** (2018).
- [67] C. L. Latune, I. Sinayskiy, and F. Petruccione, Apparent temperature: demystifying the relation between quantum coherence, correlations, and heat flows, *Quantum Science and Technology* **4**, 025005 (2019).
- [68] J. Liu and D. Segal, Coherences and the thermodynamic uncertainty relation: Insights from quantum absorption refrigerators., *Phys. Rev. E* **151** (2021).
- [69] V. Holubec and T. Novotný, Effects of noise-induced coherence on the fluctuations of current in quantum absorption refrigerators., *J. Chem. Phys.* **151** (2019).
- [70] R. Alicki, The quantum open system as a model of the heat engine, *Journal of Physics A: Mathematical and General* **12**, L103 (1979).
- [71] G. Manzano, J. M. Horowitz, and J. M. R. Parrondo, Quantum fluctuation theorems for arbitrary environments: Adiabatic and nonadiabatic entropy production, *Phys. Rev. X* **8**, 031037 (2018).
- [72] G. Manzano and R. Zambrini, Quantum thermodynamics under continuous monitoring: A general framework, *AVS Quantum Science* **4**, 025302 (2022).
- [73] A. Hewgill, G. De Chiara, and A. Imparato, Quantum thermodynamically consistent local master equations, *Phys. Rev. Res.* **3**, 013165 (2021).
- [74] P. Strasberg, G. Schaller, T. Brandes, and M. Esposito, Quantum and information thermodynamics: A unifying framework based on repeated interactions, *Phys. Rev. X* **7**, 021003 (2017).
- [75] G. Manzano, R. Sánchez, R. Silva, G. Haack, J. B. Brask, N. Brunner, and P. P. Potts, Hybrid thermal machines: Generalized thermodynamic resources for multitasking, *Phys. Rev. Res.* **2**, 043302 (2020).
- [76] R. López, J. S. Lim, and K. W. Kim, Optimal superconducting hybrid machine, *Phys. Rev. Res.* **5**, 013038 (2023).
- [77] K. Hammam, G. Manzano, and G. De Chiara, Quantum coherence enables hybrid multitask and multisource regimes in autonomous thermal machines, *Phys. Rev. Res.* **6**, 013310 (2024).
- [78] M. Esposito, U. Harbola, and S. Mukamel, Nonequilibrium fluctuations, fluctuation theorems, and counting statistics in quantum systems, *Rev. Mod. Phys.* **81**, 1665 (2009).
- [79] M. Bruderer, L. D. Contreras-Pulido, M. Thaller, L. Sironi, D. Obreschkow, and M. B. Plenio, Inverse counting statistics for stochastic and open quantum systems: the characteristic polynomial approach, *New Journal of Physics* **16**, 033030 (2014).
- [80] E. Goodarzi, M. Ziaei, and E. Z. Hosseinipour, *Introduc-*

- tion to Optimization Analysis in Hydrosystem Engineering* (Springer International Publishing, 2014).
- [81] P. P. Hofer, J.-R. Souquet, and A. A. Clerk, Quantum heat engine based on photon-assisted cooper pair tunneling, *Phys. Rev. B* **93**, 041418 (2016).
- [82] G. T. Landi, M. J. Kewming, M. T. Mitchison, and P. P. Potts, Current fluctuations in open quantum systems: Bridging the gap between quantum continuous measurements and full counting statistics (2024), [arXiv:2303.04270 \[quant-ph\]](https://arxiv.org/abs/2303.04270).
- [83] S. Pal, S. Saryal, D. Segal, T. S. Mahesh, and B. K. Agarwalla, Experimental study of the thermodynamic uncertainty relation, *Phys. Rev. Res.* **2**, 022044 (2020).
- [84] G. Schaller, *Open Quantum Systems Far from Equilibrium* (Springer International Publishing, 2014).